

THESIS

INTERNAL HYDRAULICS OF BAFFLED DISINFECTION CONTACT TANKS  
USING COMPUTATIONAL FLUID DYNAMICS

Submitted by

Qing Xu

Department of Civil and Environmental Engineering

In partial fulfillment of the requirements

For the Degree of Master of Science

Colorado State University

Fort Collins, Colorado

Summer 2010

COLORADO STATE UNIVERSITY

February 18, 2010

WE HEREBY RECOMMEND THAT THE THESIS PREPARED UNDER OUR SUPERVISION BY QING XU ENTITLED INTERNAL HYDRAULICS OF BAFFLED DISINFECTION CONTACT TANKS USING COMPUTATIONAL FLUID DYNAMICS BE ACCEPTED AS FULFILLING IN PART REQUIREMENTS FOR THE DEGREE OF MASTER OF SCIENCE.

Committee on Graduate Work

---

David Gilkey

---

Advisor: Subhas Karan Venayagamoorthy

---

Co-Advisor: Neil Grigg

---

Department Head: Luis Garcia

## ABSTRACT OF THESIS

### INTERNAL HYDRAULICS OF BAFFLED DISINFECTION CONTACT TANKS USING COMPUTATIONAL FLUID DYNAMICS

The present study focuses on understanding the internal hydraulics of baffled disinfection contact tanks for small drinking water systems using computational fluid dynamics (CFD). The emphasis of this study is to improve the hydraulic efficiency of disinfection contact tanks. In particular, the answer to the following key question was sought: for a given footprint of a contact tank, how does the hydraulic efficiency of the tank depend on the number and geometry of internal baffles? In an effort to address this question, high resolution two-dimensional (planar) simulations were performed to quantify the efficiency of a laboratory scale tank as a function of the number of baffles. Simulation results of the velocity field highlight dead (stagnant) zones in the tank that occur due to flow separation around the baffles. Simulated longitudinal velocity profiles show good agreement with previous experimental results. Analysis of residence time distribution (RTD) curves obtained for different number of baffles for a given footprint of a tank indicate that there may be an optimum number of baffles for which near plug flow conditions is maximized. This study highlights the increasing role and value of CFD in improving hydraulic design characteristics of water engineering structures. As a precursor to the CFD study, a focused literature review of disinfection systems was done

to highlight the basic technologies and related applications. The review presented in this thesis summarizes details of small water treatment plants, disinfection and  $CT$  (where  $C$  is the concentration of disinfectant at the outlet of the disinfection system, and  $T$  is the time taken for the fluid to leave the system.) method, traditional tracer studies, tank design, and the development of numerical simulations. Following the review, the CFD model used for this investigation was validated using results from a previous case study of a large-scale water treatment plant in Canada. This initial CFD study is also used to highlight the uses and abuses of CFD in flow modeling and emphasize the importance of having adequate validation studies to complement the CFD work.

Qing Xu  
Department of Civil and Environmental Engineering  
Colorado State University  
Fort Collins, CO 80523  
Summer 2010

## ACKNOWLEDGEMENTS

I would like to give special thanks to my advisor, Professor Karan Venayagamoorthy, for his guidance and support throughout the past one and a half years. His never-ending patience and knowledge has helped me immensely and I can not thank him enough. I would also like to thank my co-advisor, Professor Neil Grigg and my thesis committee member, Professor David Gilkey for their insights and valuable comments for this project.

In addition, I want to thank the great friends I have made over the past two years for always being there for me. Last but certainly not least, I would like to thank all of my family for their love and support throughout my life. To my parents: thank you for always being there for me. Even though I live 10,000 miles away, a day does not go without me realizing how much you love me, and I can not thank you enough for that

This work was supported by the Colorado Department of Public Health and Environment (CDPHE), USA (CDPHE Water Quality Program Manager: Tyson Ingels, and Program Engineers: Melanie Criswell, Gordon Whittaker and Sharon Williams). Control Division provided the scope of the project.

## TABLE OF CONTENTS

CHAPTER 1	INTRODUCTION .....	1
1.1	Introduction .....	1
1.2	Project Background .....	2
1.3	Objective .....	3
1.4	Thesis Layout .....	4
1.5	New Contributions .....	6
1.6	Research Publications.....	6
1.7	Summary .....	7
CHAPTER 2	LITERATURE REVIEW .....	8
2.1	Introduction .....	8
2.2	Water Treatment Research .....	8
2.3	Contact time and hydraulic efficiency.....	13
2.4	Tank Designs .....	14
2.5	Tracer Study Considerations .....	16
2.6	Tracer study methods .....	20
2.7	Tracer selection .....	24
2.8	Test procedure .....	26
2.9	Computational fluid dynamics (CFD) Methods.....	27
2.10	Advantages of hydraulic modeling.....	32
2.11	CFD Software.....	33
2.12	Conclusions .....	37
CHAPTER 3		
	FLOW AND TRACER MODELING IN DISINFECTION TANKS USING COMPUTATIONAL FLUID DYNAMICS .....	39
3.1	Introduction .....	39

3.2 Background .....	40
3.3 Problem statement .....	42
3.4 Numerical solutions and results in FLUENT .....	43
3.5 Comparison of particle tracking and pathlines .....	54
3.6 Summary .....	54
CHAPTER 4	
HYDRAULIC EFFICIENCY OF BAFFLED DISINFECTION TANKS .....	56
4.1 Introduction .....	56
4.2 Problem statement .....	56
4.3 Numerical framework.....	57
4.4 Results and discussions .....	60
4.5 Conclusions .....	73
CHAPTER 5 SUMMARY AND CONCLUSIONS .....	
5.1 Summary of investigations .....	75
5.2 Main conclusions.....	75
5.3 Suggestions for future research .....	76
REFERENCES .....	78
APPENDIX A – Fluoride and Lithium Tracer Study Protocol .....	81
APPENDIX B – Derivation of Reynolds Stress and RANS Equations.....	90
APPENDIX C – UDF Code using in FLUENT .....	94
APPENDIX D – Results Table of Chapter 4.....	96

## LIST OF FIGURES

Figure 2.1: Small Water Treatment Plant .....	11
Figure 2.2: The numerical scheme used to determine RTD-curve in FLUENT .....	35
Figure 3.1: The normalized barium concentration profile in Templeton’s paper for the Britannia WWP (Ottawa, Ont.) clearwell I effluent sampling location. ....	42
Figure 3.2: Example particle tracks through Britannia WWP (Ottawa, Ont.) clearwell I	43
Figure 3.3: Number of mesh faces inside the grid versus the maximum velocity of the simulations in clearwell II. ....	45
Figure 3.4: Grid independent studies of clearwell II. ....	46
Figure 3.5: Shape of cells inside the grid versus the maximum velocity of the simulations in clearwell II.....	46
Figure 3.6(a): The unstructured computational mesh for clearwell I in Britannia WWP (Ottawa, Ont.).....	47
Figure 3.6(b): Zoomed view of the mesh near the clearwell outlet area for clearwell I in Britannia WWP (Ottawa, Ont.).....	47
Figure 3.7(a): Simulated Steady-state planar velocity field in clearwell I of Britannia WWP (Ottawa, Ont.) .....	49
Figure 3.7(b): Simulated steady-state pathline contour in clearwell I of Britannia WWP (Ottawa, Ont.).....	49
Figure 3.8(a)-(h): Time sequence showing the scalar concentration in clearwell I introduced as a step dosage .....	51
Figure 3.9: RTD curve at the outlet when the tracer is injected as a step dosage.....	52
Figure 3.10: RTD curve at the outlet when the tracer is injected as a step dosage.....	53
Figure 4.1: Schematic showing the footprint of the contact tank with 7 baffles used in the simulations for this study. ....	57
Figure 4.2: Number of cells inside the grid versus the maximum velocity of the simulations in the seven-baffle tank.....	58

Figure 4.3(a): The unstructured computational mesh for the seven-baffled contact tank ... simulations.....	59
Figure 4.3(b): Zoomed view of the mesh near the tank inlet area. for the seven-baffled contact tank.....	59
Figure 4.4(a): Steady-state planar velocity field simulated in the seven-baffled tank.....	61
Figure 4.4(b): Turbulent dynamic eddy viscosity simulated in the seven-baffled tank...	61
Figure 4.5: Comparison of computed longitudinal velocity with experimental velocity data along a cross-section in compartment 5.....	62
Figure 4.6(a)-(l): Scalar concentrations in the 7-baffles tank as a step dosage .....	63
Figure 4.7: Simulated RTD curve of tracer at the outlet for the seven baffle tank as a step trace input at the inlet. ....	64
Figure 4.8(a)-(b): Scalar contours in the seven-baffle tank at $T_{10}$ and $T_{90}$ .....	65
Figure 4.9(a)-(k): Steady state velocity distributions in tanks with the number of baffles from 0 to 10. ....	66
Figure 4.10: Simulated RTD curves of tracer at the outlet with baffle numbers from 0 to 10 for a step trace input at the inlet. ....	67
Figure 4.11(a): Baffle factors as a function of the number of baffles.....	68
Figure 4.11(b): The change in baffle factor as a function of number of baffles.....	68
Figure 4.12(a): $T_m$ , $T$ and $dT$ values as a function of the number of baffles.....	71
Figure 4.12(b): $V$ , $V_m$ and $dV$ values as a function of the number of baffles. ....	71
Figure 4.13(a)-(d): Velocity contours with four different flow rates at the inlet.....	72
Figure 4.14: Baffle factors as a function of flow rate for the six-baffled tank. ....	73

## LIST OF TABLES

Table 1.1: Baffling classifications according to IESWTR.....	3
Table 1.2: Scope and purpose of each chapter.....	5
Table 2.1: Water System Categories.....	9
Table 3.1: Grid independence study on Clearwell I .....	44
Table 4.1: Grid independence study on 7 baffles tank.....	58
Table 4.2: Dead zone predictions.....	70

## **CHAPTER 1 INTRODUCTION**

### **1.1 Introduction**

Many centuries before the advent of modern science it was already known that water taken from streams could cause illness. Faust and Ally (1999) report that disinfection methods can be verified back to around 2000 BC where the Sanskrit advised that water should be boiled by dipping a hot copper rod seven times into the water or by exposing the water to sunlight. After boiling and exposure to the sun, the water should be filtered through charcoal. It was not until the 17<sup>th</sup> century that scientists were able to explain why illnesses resulted from consuming contaminated water (Faust and Ally 1999).

In 1881, Robert Koch made a remarkable discovery when he showed that chlorine could kill waterborne bacteria. Some consider this as the single most dramatic accomplishment in public health. Shortly after this discovery factories were constructed to produce chlorine on a large scale. To date, chlorine remains the dominant disinfectant used across the world, while other disinfectants such as ozone and ultraviolet (UV) are being used more frequently as an alternative and supplement to traditional method.

A great deal of effort has gone into research and development of simple and effective theories and models in disinfection tanks. Publications in this field are broad encompassing fundamental aspects to the more specific application in engineering. This thesis will investigate the background of this project, introduce the traditional tracer study

approach for contact tank design, and describe how contact tank hydraulics can be better understood using CFD in an effort to improve tank design. It should be noted that even though the focus of this study is on disinfection tanks, the concepts and principles can be easily extended to other mixing tanks such as clarifiers and sedimentation tanks in water and wastewater treatment.

## **1.2 Project Background**

Currently, the Water Quality Control Division of the Colorado Department of Public Health and Environment (CDPHE) is evaluating the disinfection log inactivation as part of the Ground Water Rule implementation process and future State of Colorado Design Criteria for Potable Water System (Design Criteria) revisions. Under the recently promulgated Ground Water Rule, groundwater systems will have stricter regulatory oversight. Those systems that can demonstrate 4-log inactivation of viruses are exempt from the triggered source water monitoring. Furthermore, systems with susceptible groundwater sources will be required to demonstrate 4-log inactivation of viruses or they will have to install a system upgrade with an approved design.

Colorado's water utilities currently determine the disinfection log inactivation using the protocol described in the United States Environmental Protection Agency (USEPA), 1999, LTIESWTR (Long Term 1 Enhanced Surface Water Treatment Rules) Disinfection Profiling and Benchmarking Technical Guidance Manual. The EPA document has a general baffling factor description chart (see Table 1.1 below) and some example baffling configurations.

**Table 1.1: Baffling classifications according to IESWTR (1999)**

Baffling Condition	$T_{10}/T$	Baffling Description
Unbaffled (mixed flow)	0.1	None, agitated basin, very low length to width ratio, high inlet and outlet flow velocities.
Poor	0.3	Single or multiple unbaffled inlets and outlets, no intra-basin baffles.
Average	0.5	Baffled inlet or outlet with some intra-basin baffles.
Superior	0.7	Perforated inlet baffle, serpentine or perforated intra-basin baffles, outlet weir or perforated launders.
Perfect (plug flow)	1.0	Very high length to width ratio (pipeline flow), perforated inlet, outlet, and intra-basin baffles.

The contact basin baffling factors in EPA document are potentially imprecise factors in the log inactivation calculation. Furthermore, the EPA baffling conditions have limited applicability for the contact tanks configurations utilized by many small public water systems in Colorado.

### **1.3 Objective**

The purpose of this study is to increase current knowledge on disinfection baffling factors and to use the acquired knowledge to provide technical assistance to small system to comply with disinfection requirements.

The entire scope for this study includes three phases:

- Phase 1: Literature review on disinfection tanks and their internal hydraulics;
- Phase 2: CFD validation with field data in water treatment plant;
- Phase 3: Study on hydraulic efficiency of small-scale disinfection contact tanks.

The first phase of the study will be to analyze and summarize the existing knowledge and potential analysis tools for disinfection tanks. This portion of the study will assemble

technical resources to enable us to decide on how to effectively ensure that Colorado's water utilities provide sufficient disinfection log inactivation to meet the Colorado Primary Drinking Water Regulation.

The purpose of Phase 2 is to develop and validate a CFD model using results obtained from tracer studies of a large scale water treatment tank.

In phase 3, we implement a research project on disinfection system design for a given footprint of a small-scale disinfection contact tank, as an example for further research of disinfection tank design. The goal is to create several tank configurations using CFD and analyze the hydraulic efficiency of these tanks in order to determine the optimal design.

#### **1.4 Thesis Layout**

The technical content of this thesis has been arranged into four further chapters and two appendices. Chapter 2 presents the literature review summary of phase 1. Definitions of the basic parameters used in the context of this research are provided together with the equation of motion governing such situations. Review on work done on hydraulic efficiency of disinfection tanks used in water and wastewater treatment plants is presented and observations drawn.

In Chapter 3, a CFD study of a previous published work on water treatment tanks is used to demonstrate how CFD works. A discussion on how to computationally simulate a tracer is given in order to explain how CFD can be abused if it is used wrongly.

Chapter 4 presents the innovative part of this thesis in that it presents the study on understanding the internal hydraulic efficiency of baffled disinfection contact tanks and

highlights the increasing role and value of CFD in improving hydraulic design characteristics of water treatment structures.

Chapter 5 concludes this thesis by summarizing what has been done and the main findings thereof in this study. Directions on future work from the author’s point of view waiting in this exciting and important field are indicated.

Appendix A provides a protocol for Lithium and Fluoride tracer studies that was developed from a tracer study done on a pipe loop at the City of Fort Collins Water Treatment works. Appendix B provides the details of the derivation of the Reynolds averaged Navier-Stokes equations (RANS). Appendix C provides additional details of the FLUENT code and details for the modeling the scalar turbulent diffusivity and finally, Appendix D provides tables of results presented in Chapter 4.

Table 1.2 depicts the schematic flow of the chapters.

**Table 1.2: Scope and purpose of each chapter**

Scope and purpose of chapter	
Chapter 1	Introduction to objective and purpose of the study
Chapter 2	Literature review to gain insight into the problem of water disinfection and understanding of existing technology
Chapter 3	Application of CFD to a published contact tank study to introduce the modeling tool and highlight some of the shortcoming of not accounting for the correct physics.
Chapter 4	Application of CFD to understanding the internal hydraulic efficiency of baffled disinfection contact tanks and highlight the increasing role and value of CFD in improving hydraulic design characteristics of water treatment systems.
Chapter 5	Summary and discussion of the contributions and directions for future study.

## **1.5 New Contributions**

While the work of this thesis is primarily an extension of the work of others (Wang et al 1998), it nevertheless makes the following meaningful and original contributions to research on disinfection tanks.

- It uses existing field tracer test data to validate a CFD model and understand the internal hydraulic efficiency of contact tanks.
- It uses widely used commercial CFD software is used to solve the internal hydraulics and turbulent mixing problem within a disinfection tank and explain the process in detail. This is more practical for applications in industry as opposed to using a user written research code.
- It demonstrates that the ability to predict dead zones inside a disinfection tank using CFD is valuable in determine the optimal design of a disinfection tank for a given footprint.

## **1.6 Research Publications**

Paper on some aspects and findings of the work of this thesis has been accepted to presentation at the 6th International of Symposium Environmental Hydraulics (Xu and Venayagamoorthy 2010).

An extended version of this article is currently under preparation for submission to the Journal of Environmental Engineering, American Society of Civil Engineers.

## **1.7 Summary**

This thesis investigates primarily the internal hydraulics of baffled disinfection contact tanks. The investigation is carried out by means of CFD using the commercial software FLUENT.

The main body of this thesis starts in the next chapter which provides a brief literature review on disinfection contact tanks.

## **CHAPTER 2 LITERATURE REVIEW**

### **2.1 Introduction**

The goal of this initial chapter is to perform a literature review on the contact tank baffling factors. This literature review discusses water treatment research, contact time and tank characteristics, tracer studies, modeling methods and software.

### **2.2 Water Treatment Research**

#### **2.2.1 Small Water Treatment Facilities**

The term “small water systems” differs in meaning throughout the world. The United States Environmental Protection Agency (USEPA) defines a small system as one that serves a population of fewer than 3,300 people. Definitions may differ even between federal agency involves. For example, the USGS defines a small system as one that serves fewer than 10,000 people. The province of British Columbia, Canada, has a tiered classification for small water systems based on the number of connections, as follows:

- WS4: 1 connection, semi-public; i.e., restaurant/ resort/gas station
- WS3: 2-15 connections
- WS2: 16-300 connections
- WS1a: 301-10,000 connections
- WS1b: 10,001-20,000 connections
- WS1c: more than 20,000 connections.

In USEPA document (Small Water System Byproducts Treatment and Disposal Cost Document 1993), water systems are identified to 12 categories. As shown in Table 2.1, small water systems include systems in Categories 1 through Categories 4.

In effect, the issues under discussion relate more to the availability of resources and operating characteristics than to the actual size of the system. Therefore a small system may be defined as one that has pressing limitation in terms of resource and technology available to produce and monitor for “safe” water.

**Table 2.1: Water System Categories**

Category	Population Range	Median Population	Average Flow (MGD)	Design Flow (MGD)
1	25-100	57	0.0056	0.024
2	101-500	225	0.024	0.087
3	501-1000	750	0.086	0.27
4	1001-3300	1910	0.23	0.65
5	3301-10000	5500	0.7	1.8
6	10001-25000	15500	2.1	4.8
7	25001-50000	35500	5	11
8	50001-75000	60000	8.8	18
9	75001-100000	88100	13	26
10	100001-500000	175000	27	51
11	500001-1000000	730000	120	210
12	Greater than 1000000	1550000	270	430

Source: Office of Ground Water & Drinking Water, U.S. EPA

### *Background*

There are approximately 160,000 small community and non-community drinking water treatment systems in the United States. Approximately 50,000 small community systems and 110,000 non-community systems provide drinking water for more than over 68 million people (USEPA Safe Drinking Water Act Amendments of 1996 and Understanding the Safe Drinking Water Act 2003). However, countless small drinking

water systems serve transient and non-transient populations of 10,000 people or less. Tens of thousands of the small systems are having difficulty complying with the ever-increasing number of regulations and regulated contaminants.

Currently, 94 percent of the Safe Drinking Water Act (SDWA) annual violations are attributed to small systems. Nearly 77% of these are for Maximum Contaminant Level (MCL) violations, often directly related to microbiological violations. The EPA conducts in-house technology development and evaluation to support small communities, in addressing the cause of these violations. The EPA makes this information is to the small system operators, consultants, and utilities. Disinfection technology for small water treatment system is the most important element in addressing quality concerns. Figure 2.1 shows a treating process of a small water treatment plant (Report of the national drinking water advisory council small water systems implementation working group, USEPA 2000).

### *Disinfection*

Historically chlorine has been the world's most widely used disinfectant, as shown by White (1998), chlorination of drinking waters has become a worldwide practice, shortly after the chemical was first used as a germicide in the 19<sup>th</sup> century. However, with the discovery of health hazardous disinfection by-products (DBPs) in the 1970s, other technologies have been developed and applied for disinfection purposes, such as ozonation, ultraviolet radiation and ultrasonics. These technologies have not generally replaced chlorine's near universal use, either as the sole disinfectant in a water treatment plant or in conjunction with other technologies.

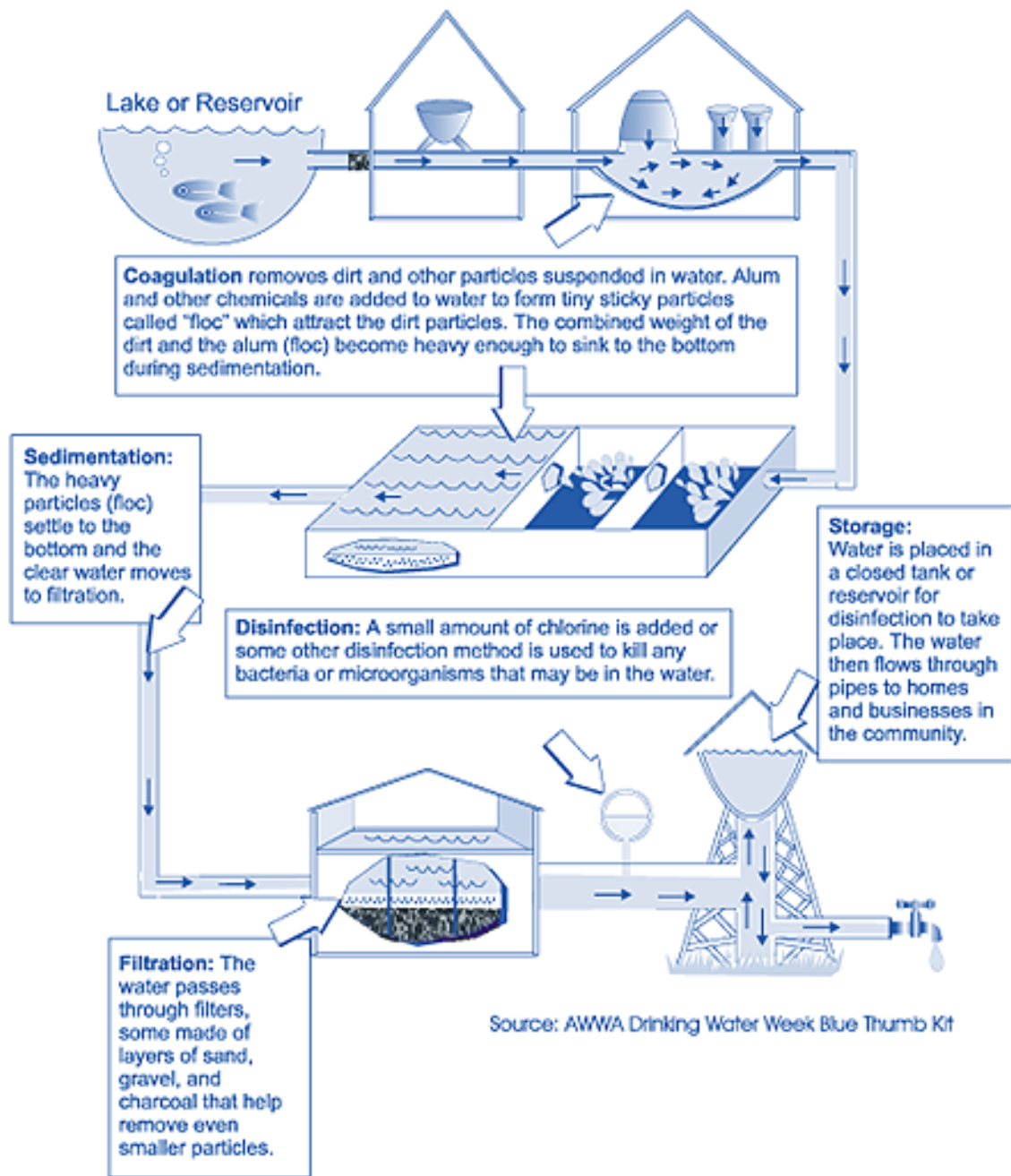


Figure 2.1: Small Water Treatment Plant  
(USEPA Drinking Water Treatment document, 2004)

The objective of a contact tank is to bring as much water into contact with chlorine for as long as possible to achieve a certain level of disinfection to prevent the transmission of water-borne diseases. Disinfection is influenced by a number of variables

such as the disinfectant used, the physical quality of the water, and the biological quality of the water. Some aspects of particular importance that will be highlighted later in the chapter are:

- The transport of the water:
  - Inlet conditions
  - Flow rate and residence time
  - Velocity contours
  - Stagnant zones and recirculation zones
- Geometry of the tank:
  - Inlet geometry
  - Internal features such as baffles
  - Outlet features

Disinfection is also affected by the properties and quantity of the particulate matter in the water.

Reactions between chlorine compounds and microorganisms are very complex and time-dependent. The ideal performance of a disinfection contact tank assumes that all water packets pass through the tank with equal residence times, giving rise to an idealized flow pattern known as “plug flow”. However, since non-idealities invariably occur in practice, a disinfection contact tank should be designed to avoid short circuiting and should be as near to a plug flow system as is practicable. This is generally achieved through the use of a pipeline.

Occurrence of recirculating flow regions need to be minimized, since they tend to impair a unit's hydraulic efficiency by increasing the overall mixing levels in the flow and, consequently, causing departure of the flow pattern from plug flow.

As in the context of Teixeira (2000) findings, an optimized contact tank will generally have a flow field of a primarily 2D horizontal nature, aiming to provide: (i) the maximum level of microbial inactivation, i.e. disinfection efficiency; (ii) the minimum operational costs, e.g. with reagents; and (iii) the minimum level of CBP formation.

### **2.3 Contact time and hydraulic efficiency**

The USEPA determines the effectiveness of contact tanks for disinfection by the *CT* method. *C* is the concentration of disinfectant at the outlet of the tank and *T* is usually taken as the  $T_{10}$  value. The  $T_{10}$  value is the time required for 10% of the fluid to leave the tank, or the time at which 90% of the fluid is retained in the tank and subjected to at least a disinfectant level of *C*. A high  $T_{10}$  value will allow the treatment plant to achieve a high level of disinfection credit for a given concentration of disinfectant. The ratio of  $T_{10}$  and the theoretical hydraulic residence time (*HRT*) determines the contactor hydraulic efficiency, or baffling factor ( $BF = T_{10}/HRT$ ). The number and character of the internal baffles, inlet and outlet locations, and the contact tank geometry can influence the  $T_{10}/HRT$  factor (Crozes et al. 1998).

However, it is useful to be able to predict not just the  $T_{10}/HRT$  (baffle) factor, but also the entire residence time distribution (RTD) curve. The entire RTD curve can then be used to predict the overall microbial inactivation level as well as the formation of disinfection by-product (DBPs) (Bellamy et al. 1998, 2000; Ducoste et al. 2001). In a recent study, researchers have shown that the use of the entire RTD curve with more

appropriate microbial inactivation/DBP models could lead to a reduction in the disinfectant dose, while still maintaining the same credit for *Giardia* inactivation specified by the USEPA *CT* tables (Ducoste et al. 2001).

## **2.4 Tank Designs**

### **2.4.1 Impact of Design Characteristics**

Clearwells or disinfection contactors serve a variety of roles at water treatment plants including storage, water pressure equalization, and disinfection.

The significant design characteristics include length-to-width ratio, the degree of baffling within the basins, and the effect of inlet baffling and outlet weir configuration. These physical characteristics of the contact basins affect their hydraulic efficiencies in terms of dead space, plug flow, and mixed flow proportions. The dead space zone of a basin is the basin volume through which no flow occurs. The remaining volume where flow occurs is comprised of plug flow and mixed flow zones. The plug flow zone is the portion of the remaining volume in which no mixing occurs in the direction of flow. The mixed flow zone is characterized by complete mixing in the flow direction and is the complement to the plug flow zone. All of these zones were identified in the studies for each contact basin.

Comparisons were then made between the basin configurations and the observed flow conditions and design characteristics.

The ratio  $T_{10}/HRT$  was calculated from the data presented in the studies and compared to its associated hydraulic flow characteristics. Both studies resulted in  $T_{10}/HRT$  values that ranged from 0.3 to 0.7. The results of the studies indicate how basin baffling conditions can influence the  $T_{10}/HRT$  ratio, particularly baffling at the inlet and outlet to

the basin. As the basin baffling conditions improved, higher  $T_{10}/HRT$  values were observed, with the outlet conditions generally having a greater impact than the inlet conditions.

Marske and Boyle (1973) and Hudson (1975) showed a high  $T_{10}/HRT$  fraction is more related to the geometry and baffling of the basin than the function of the basin. For this reason,  $T_{10}/HRT$  values may be defined for five levels of baffling conditions rather than for particular types of contact basins. General guidelines were developed relating the  $T_{10}/HRT$  values from these studies to the respective baffling characteristics. These guidelines can be used to determine the  $T_{10}$  values for specific basins.

#### 2.4.2 Baffling Classifications

The purpose of baffling is to maximize utilization of basin volume, increase the plug flow zone in the basin, and minimize short-circuiting. Ideal baffling design reduces the inlet and outlet flow velocities, distributes the water as uniformly as practical over the cross section of the basin, minimizes mixing with the water already in the basin, and prevents entering water from short-circuiting to the basin outlet as the result of wind or density current effects.

Some form of baffling at the inlet and outlet of the basins is used to evenly distribute flow across the basin. Additional baffling may be provided within the interior of the basin (intra-basin) in circumstances requiring a greater degree of flow distribution.

Five general classifications of baffling conditions - unbaffled, poor, average, superior, and perfect (plug flow) - were developed to categorize the results of the tracer studies for use in determining  $T_{10}$  from the TDT of a specific basin. Table 1.1 contains these classifications.

The  $T_{10}/HRT$  fractions associated with each degree of baffling are summarized in Table 1.1. However, in practice the theoretical  $T_{10}/HRT$  values of 1.0 for plug flow and 0.1 for mixed flow are seldom achieved because of the effect of dead space. Conversely, the  $T_{10}/HRT$  values shown for the intermediate baffling conditions already incorporate the effect of the dead space zone, as well as the plug flow zone, because they were derived empirically rather than from theory.

The three basic types of basin inlet baffling configurations are a target-baffled pipe inlet, an overflow weir entrance, and a baffled submerged orifice or port inlet. Typical intra-basin baffling structures include diffuser (perforated) walls; launders; cross, longitudinal, or maze baffling to cause horizontal and/or vertical serpentine flow; and longitudinal divider walls, which prevent mixing by increasing the length-to-width ratio of the basin(s). Commonly used baffled outlet structures include free-discharging weirs, such as sharp-crested and multiple V-notch, and submerged ports or weirs. Weirs that do not span the width of the contact basin, such as Cipolletti weirs, should not be considered for baffling as their use may substantially increase weir overflow rates and the dead space zone of the basin.

## **2.5 Tracer Study Considerations**

A tracer study uses a conservative chemical to track flow patterns and hydraulic residence times to determine the degree of internal mixing or short circuiting. The chemical is added prior to one or more unit processes, and the process effluent is monitored over time until a steady state in chemical concentration is observed.

### 2.5.1 Flow Evaluation

Ideally, tracer tests should be performed for at least four flow rates that span the entire range of flow for the segment being tested. The flow rates should be separated by approximately equal intervals to span the range of operation, with one near average flow, two greater than average, and one less than average flow. The flows should also be selected so that the highest test flow rate is at least 91 percent of the highest flow rate expected to ever occur in that segment. Four data points should assure a good definition of the segment's hydraulic profile.

It may not be practical for all systems to conduct studies at four flow rates. The number of tracer tests that are practical to conduct is dependent on site-specific restrictions and resources available to the system. Systems with limited resource can conduct a minimum of one tracer test for each disinfectant segment at a flow rate of not less than 91 percent of the highest flow rate experienced at that segment.

The most accurate tracer test results are obtained when flow is constant through the segment during the course of the test. Therefore, the tracer study should be conducted at a constant flow rate whenever practical.

For a treatment plant consisting of two or more equivalent process trains, a constant flow tracer test can be performed on a segment of the plant by holding the flow through one of the trains constant while operating the parallel train(s) to absorb any flow variations. Flow variations during tracer tests in systems without parallel trains or with single clearwells and storage reservoirs are more difficult to avoid. In these instances,  $T_{10}$  should be recorded at the average flow rate over the course of the test.

### 2.5.2 Volume Evaluation

In addition to flow conditions, detention times determined by tracer studies depend on the water level and subsequent volume in treatment units.

This is particularly pertinent to storage tanks, reservoirs, and clearwells, which, in addition to being contact basins for disinfection are also often used as equalization storage for distribution system demands and storage for backwashing. In such instances, the water levels in the reservoirs vary to meet the system demands. The actual detention time of these contact basins will also vary depending on whether they are emptying or filling.

For some process units, especially sedimentation basins that are operated at a near constant level (that is, flow in equals flow out), the detention time determined by tracer tests should be sufficient for calculating *CT* when the basin is operating at water levels greater than or equal to the level at which the test was performed. If the water level during testing is higher than the normal operating level, the resulting concentration profile will predict an erroneously high detention time. Conversely, extremely low water level during testing may lead to an overly conservative detention time. Therefore, when conducting a tracer study to determine the detention time, a water level at or slightly below, but not above, the normal minimum operating level is recommended.

For many plants, the water level in a clearwell or storage tank varies between high and low levels in response to distribution system demands. In such instances, in order to obtain a conservative estimate of the contact time, the tracer study should be conducted during a period when the tank level is falling (flow out greater than flow in).

### 2.5.3 Disinfection Segments

For systems that apply disinfectants at more than one point, or choose to profile the residual from one point of application, tracer studies should be conducted to determine  $T_{10}$  for each segment containing a process unit. The  $T_{10}$  for a segment may or may not include a length of pipe and is used along with the residual disinfectant concentration prior to the next disinfectant application or monitoring point to determine the  $CT$  for that segment. The inactivation ratio for the section is then determined. The total log inactivation achieved in the system can then be determined by summing the inactivation ratios for all sections.

For systems that have two or more units of identical size and configuration, tracer studies could be conducted on one of the units but applied to both. The resulting graph of  $T_{10}$  versus flow can be used to determine  $T_{10}$  for all identical units. Systems with more than one segment in the treatment plant that are conducting a tracer study may determine  $T_{10}$  for each segment:

- By individual tracer studies through each segment; or,
- By one tracer study across the system.

If possible, tracer studies should be conducted on each segment to determine the  $T_{10}$  for each segment. In order to minimize the time needed to conduct studies on each segment, the tracer studies should be started at the last segment of the treatment train prior to the first customer and completed with the first segment of the system. Conducting the tracer studies in this order will prevent the interference of residual tracer material with subsequent studies.

For ozone contactors, flocculators or any basin containing mixing, tracer studies should be conducted for the range of mixing used in the process. In ozone contactors, air or oxygen should be added in lieu of ozone to prevent degradation of the tracer. The flow rate of air or oxygen used for the contactor should be applied during the study to simulate actual operation. Tracer studies should then be conducted at several air/oxygen to water ratios to provide data for the complete range of ratios used at the plant. For flocculators, tracer studies should be conducted for various mixing intensities to provide data for the complete range of operations.

#### 2.5.4 Other Considerations

Detention time may also be influenced by differences in water temperature within the system. For plants with potential for thermal stratification, additional tracer studies are suggested under the various seasonal conditions that are likely to occur.

### 2.6 Tracer study methods

There are two most common methods of tracer addition employed in water treatment evaluations: the step-dose method and the slug-dose method. The slug or pulse input requires “instantaneous” introduction of the entire chemical mass, and is not easily applied to enclosed or pressurized systems. Step input requires the continuous introduction of a known chemical concentration at a constant dosage.

In general, the step-dose procedure offers the greatest simplicity. However, both methods are theoretically equivalent for determining  $T_{10}$ . While either method is acceptable for conducting drinking water tracer studies, each has distinct advantages and

disadvantages with respect to tracer addition procedures and analysis of results. The choice of the method may be determined by site-specific constraints.

### 2.6.1 Step-Dose Method

The step-dose method entails introduction of a tracer chemical at a constant dosage until the concentration at the desired end reaches a steady-state level. At time zero, the tracer chemical injection is started and left at a constant rate for the duration of the test. Over the course of the test, the tracer residual should be monitored at the required sampling points at a frequency determined by the overall detention time and site-specific considerations. As a general guideline, sampling at intervals of 2 to 5 minutes should provide data for a well-defined plot of tracer concentration versus time (i.e. the RTD curve).

If on-site analysis is available, less frequent residual monitoring may be possible until a change in residual concentration is first detected. Regular sampling is continued until the residual concentration reaches a steady-state value. One graphical method of evaluating step-dose test data involves plotting a graph of dimensionless concentration ( $C/C_0$  where  $C$  is the tracer concentration at the sampling point and  $C_0$  is the input tracer concentration) versus time. This way, the value for  $T_{10}$  can be directly read from the graph at the appropriate dimensionless concentration.

Alternatively, the data from step-dose tracer studies may be evaluated numerically by developing a semi-logarithmic plot of the dimensionless data. The semi-logarithmic plot allows a straight line to be drawn through the data. The resulting equation of the line is used to calculate the  $T_{10}$  value, assuming that the correlation coefficient indicates a good statistical fit (0.9 or above). Drawing a smooth curve through the data discredits

scattered data points from step-dose tracer tests. Step-dose tracer studies are frequently employed in drinking water applications for the following reasons:

- The resulting normalized concentration versus time profile is directly used to determine  $T_{10}$ , the detention time required for calculating  $CT$ ; and,
- Very often, the necessary feed equipment is available to provide a constant rate of application of the tracer chemical.

One other advantage of the step-dose method is that the data may be verified by comparing the concentration versus elapsed time profile for samples collected at the start of dosing with the profile obtained when the tracer feed is discontinued.

### 2.6.2 Slug-Dose Method

In the slug-dose method, a large instantaneous dose of tracer is added to the incoming water and samples are taken at the exit of the unit over time as the tracer passes through the unit. The same sampling locations and frequencies described for step-dose method tests also apply to slug-dose method tracer studies. One important exception with this method is that the tracer concentration profile will not equilibrate to a steady-state concentration. Because of this, frequent monitoring is necessary to ensure acquisition of data needed to identify the peak tracer concentration.

Slug-dose method tests should be checked by performing a mass balance to ensure that the entire tracer feed is recovered or mass applied equals mass discharged.

Data from slug-dose tracer tests may be analyzed by converting it to the mathematically equivalent step-dose data and using the techniques discussed above for the step-dose method to determine  $T_{10}$ . A graph of dimensionless concentration versus time should be drawn which represents the results of a slug-dose tracer test. The key to

converting between the different data forms is the total area under the slug-dose data curve. This area is found by integrating the curve graphically or numerically. The conversion to step-dose data is then completed in several mathematical steps involving the total area.

Slug-dose concentration profiles can have many shapes, depending on the hydraulics of the basin. Therefore, slug-dose data points should not be discredited by drawing a smooth curve through the data prior to its conversion to step-dose data.

A disadvantage of the slug-dose method is that very concentrated solutions are needed for the dose in order to adequately define the concentration versus time (or the RTD) profile. Intensive mixing is therefore necessary to minimize potential density-current effects and to obtain a uniform distribution of the instantaneous tracer dose across the basin. This is inherently difficult under water flow conditions often existing at inlets to basins. Other disadvantages of using the slug-dose method include:

- The concentration and volume of the instantaneous tracer dose needs to be carefully computed to provide an adequate tracer profile at the effluent of the basin;
- The resulting concentration versus time profile should not be used to directly determine  $T_{10}$  without further manipulation; and,
- A mass balance on the treatment segment should be used to determine whether the tracer was completely recovered.

One advantage of this method is that it may be applied where chemical feed equipment is not available at the desired point of addition, or where the equipment available does not have the capacity to provide the necessary concentration of the chosen tracer chemical.

## 2.7 Tracer selection

An important step in any tracer study is the selection of a chemical to be used as the tracer. Ideally, the selected tracer chemical should be readily available, conservative (i.e. a chemical that is not reactive or removed during treatment), easily monitored, and acceptable for use in potable water supplies. Chlorides and Fluorides are the most common tracer chemicals employed in drinking water plants since they are low toxicity to humans and are approved for potable water use. Rhodamine WT (water tracing) can be used as a fluorescent tracer in water flow studies in accordance with the following guidelines:

- Raw water concentrations should be limited to a maximum concentration of 10 mg/L;
- Drinking water concentrations should not exceed 0.1 µg/L;
- Studies that result in human exposure to the dye should be brief and infrequent; and,
- Concentrations as low as 2 µg/L can be used in tracer studies because of the low detection level in the range of 0.1 to 0.2 µg/L.

The use of Rhodamine B as a tracer in water flow studies is not recommended by the EPA. The choice of a tracer chemical can be made based, in part, on the selected dosing method and on the availability of chemical feeding equipment. For example, the high density of concentrated salt solutions and their potential for inducing density currents usually precludes chloride and fluoride as the selected chemical for slug-dose tracer tests.

Fluoride can be a convenient tracer chemical for step-dose tracer tests of clearwells because it is frequently applied for finished water treatment. However, when fluoride is

used in tracer tests on clarifiers, allowances should be made for fluoride that is absorbed on floc and settles out of water (Hudson 1975). Additional considerations when using fluoride in tracer studies include:

- It is difficult to detect at low levels,
- Many states impose a finished water limitation of 1 mg/L; and,
- The federal secondary and primary drinking water standards (i.e. the MCLs) for fluoride are 2 and 4 mg/L, respectively.

For safety reasons, particularly for people on dialysis, fluoride is not recommended for use as a tracer in systems that normally do not fluoridate their water. The use of fluoride is only recommended in cases where the feed equipment is already in place. The system may wish to turn off the fluoride feed in the plant for 12 or more hours prior to beginning the fluoride feed for the tracer study. Flushing out fluoride residuals from the system prior to conducting the tracer study is recommended to reduce background levels and avoid spiked levels of fluoride that might exceed EPA's MCL or Suggested MCL for fluoride in drinking water. In instances where only one of two or more parallel units is tested, flow from the other units would dilute the tracer concentration prior to leaving the plant and entering the distribution system. Therefore, the impact of drinking water standards on the use of fluoride and other tracer chemicals can be alleviated in some cases.

Lithium is another suitable conservative tracer that can be used in tracer studies if very accurate results are required. However, onsite monitoring of concentration profiles is not possible since advanced laboratory analysis such as atomic absorption spectroscopy (AAS) or inductively coupled plasma atomic emission spectroscopy (ICP-AES) is

required to detect concentration of the metal. However, Lithium is often a prime candidate since the only very small amount of a Lithium salt is required in a tracer studies since the background concentrations of Lithium in water is much less than 1 µg/L.

## **2.8 Test procedure**

In preparation for beginning a tracer study, the raw water background concentration of the chosen tracer chemical should be established. The background concentration is important, not only to aid in the selection of the tracer dosage, but also to facilitate proper evaluation of the data.

The background tracer concentration should be determined by monitoring for the tracer chemical prior to beginning the test. The sampling point for the pre-tracer study monitoring should be the same as the points as those used for residual monitoring to determine *CT* values. Systems should use the following monitoring procedure:

- Prior to the start of the test, regardless of whether the chosen tracer material is a treatment chemical, the tracer concentration in the water is monitored at the sampling point where the disinfectant residual will be measured for *CT* calculations.
- If a background tracer concentration is detected, monitor it until a constant concentration, at or below the raw water background level, is achieved. This measured concentration is the baseline tracer concentration.

Following the determination of the tracer dosage, feed and monitoring point(s), and a baseline tracer concentration, tracer testing can begin.

Equal sampling intervals, as could be obtained from automatic sampling, are not required for either tracer study method. However, using equal sample intervals for the slug-dose method can simplify the analysis of the data. During testing, the time and

tracer residual of each measurement should also be recorded on a data sheet. In addition, the water level, flow, and temperature should be recorded during the test.

A test plan checking list is attached in Appendix A.

## **2.9 Computational fluid dynamics (CFD) Methods**

### **2.9.1 Background**

Computational fluid dynamic (CFD) studies have been used increasingly recently to simulate and understand contact tank hydraulics. However, most CFD studies on contact tanks have focused on understanding the hydrodynamics only without simulating the tracer transport (Gualtieri 2004). The flow inside a contact tank is usually modeled on the premise that the variations of relevant quantities in the vertical direction, except in the thin boundary layer near channel bottom and possibly near the free surface, are substantially smaller than variations across the width or in streamwise direction. Thus, two-dimensional or depth-averaged models may be applied to describe hydrodynamics and mass-transfer processes. These CFD models are based on the mass conservation equation and the Navier-Stokes equations of motion. Since the flow in the tank is turbulent, these equations must be averaged over a small time increment applying Reynolds decomposition, which results in the Reynolds-averaged Navier-Stokes equations (RANS) equations. Once the flow (velocity) is computed, the resident time distribution (RTD) curves may be obtained by solving a tracer transport equation using the velocity field obtained from the solution of the Navier-Stokes equations.

### 2.9.2 Navier–Stokes Equations

The theoretical basis of CFD modeling is the Navier-Stokes fluid dynamics equations, which are used to model fluid flow parameters such as velocity, temperature, and pressure. Velocity contours can be used to trace the paths of particles that travel through the modeled unit process, which allows residence time distributions to be calculated.

The Navier–Stokes equations describe the motion of fluid parcels. These equations arise from applying Newton's second law to fluid motion, together with the assumption that the fluid stress is the sum of a diffusing viscous term (proportional to the gradient of velocity), plus a pressure term.

Equation 1 gives the general form of the Navier-Stokes equations (in tensor notation) with the Boussinesq approximation.

$$\frac{\partial u_i}{\partial t} + \frac{\partial}{\partial x_j} (u_i u_j) = -\frac{1}{\rho_0} \frac{\partial P}{\partial x_j} + \nu \frac{\partial^2 u_i}{\partial x_i \partial x_j} - \frac{g}{\rho_0} \rho \delta_{iz} \quad (2.1)$$

Where  $u_i$  is the velocity field,  $P$  is the pressure,  $\rho$  is the density of the fluid and  $\nu$  is the kinematic viscosity. The Boussinesq Approximation involves using an algebraic equation for the Reynolds stresses which include determining the turbulent viscosity, and depending on the level of sophistication of the model, solving transport equations for determining the turbulent kinetic energy and dissipation.

### 2.9.3 Turbulence and Turbulence Models

Turbulence is the time dependent chaotic behavior seen in many fluid flows. It is generally believed that it is due to the inertia of the fluid as a whole: the culmination of time dependent and convective acceleration; hence, flows where inertial effects are small tend to be laminar (the Reynolds number quantifies how much the flow is affected by

inertia). It is believed, though not known with certainty, that the Navier–Stokes equations describe turbulence properly.

The numerical solution of the Navier–Stokes equations for turbulent flow is extremely difficult, and due to the significantly different mixing-length scales that are involved in turbulent flow, the stable solution of this set of equations requires a very fine mesh resolution resulting in computational times that are prohibitively expensive. To counter this, time-averaged equations such as RANS, supplemented with turbulence models (such as the  $k$ - $\varepsilon$  model), are used in practical CFD applications for modeling turbulent flows.

Another technique for solving numerically the Navier–Stokes equation is the Large-eddy simulation (LES). This approach is computationally more expensive than the RANS method (in time and computer memory), but produces better results since the larger turbulent scales are explicitly resolved. A brief summary of the three state-of-the-art approaches to solving turbulent flow problems are provided next.

#### *Direct Numerical Simulation (DNS)*

A direct numerical simulation (DNS) solution involves a complete time-dependent solution of the Navier-Stokes and continuity equations (Wilcox 2007) without any modeling assumptions. Currently, DNS models have only provided solutions for problems involving simple geometries because of the immense power and cost required to completely solve the time-dependent Navier-Stokes and continuity equations. Analysis of disinfection contact tanks is not a viable using DNS due to the current limitations of computing power.

### *Large Eddy Simulation (LES)*

A large eddy simulation (LES) solution involves a hybrid of DNS and RANS solutions (Wilcox 2007). Solutions to the largest eddies are computed while solutions to the smallest eddies are modeled using averaged solutions. Solutions for LES still requires more computational power than RANS and orders of magnitude difference in solution time, but are becoming more feasible with increasing computing power and the corresponding decrease in price of computing power.

### *Reynolds-Averaged Navier-Stokes (RANS)*

Reynolds-averaged Navier-Stokes (RANS) equations are the oldest approach to turbulence modeling. An ensemble averaged version of the governing equations is solved, which introduces new apparent stresses known as Reynolds stresses. This adds a second order tensor of unknowns for which various models can provide different levels of closure. It is a common misconception that the RANS equations do not apply to flows with a time-varying mean flow because these equations are 'time-averaged'. In fact, statistically unsteady (or non-stationary) flows can equally be treated. This is sometimes referred to as URANS. There is nothing inherent in Reynolds averaging to preclude this, but the turbulence models used to close the equations are valid only as long as the time scale of these changes in the mean is large compared to the time scales of the turbulent motion containing most of the energy.

Reynolds-averaged Navier–Stokes (RANS) equations are time-averaged equations of motion for fluid flow. They are primarily used while dealing with turbulent flows. These equations can be used with approximations based on knowledge of the properties of flow turbulence to give approximate averaged solutions to the Navier–Stokes equations.

$$\rho \frac{\partial \overline{u_j u_i}}{\partial x_j} = \rho \overline{f_i} + \frac{\partial}{\partial x_j} \left[ -\overline{p} \delta_{ij} + \mu \left( \frac{\partial \overline{u_i}}{\partial x_j} + \frac{\partial \overline{u_j}}{\partial x_i} \right) - \rho \overline{u'_i u'_j} \right] \quad (2.2)$$

The left hand side of this equation represents the change in mean momentum of fluid element due to the unsteadiness in the mean flow and the convection by the mean flow. This change is balanced by the mean body force, the isotropic stress due to the mean pressure field, the viscous stresses, and apparent stress  $\overline{\rho u'_i u'_j}$  due to the fluctuating velocity field, generally referred to as Reynolds stresses.

The derivations for Reynolds stress and the RANS equations are found in the Appendix B.

#### *One-Equation Turbulence Models*

One faction of RANS models uses a singular differential equation to solve for the eddy, or turbulent, viscosity,  $\mu_t$  of the system. Spalart and Allmaras (1992) formulated these equations. These equations were primarily developed for flow past airfoils and were successful in that endeavor. In applications involving other flows, the Spalart and Allmaras equations have worked reasonably well.

#### *Two-Equation Turbulence Models*

The most popular of the two equation models are the  $k$ - $\epsilon$  model (Launder and Sharma 1974) and  $k$ - $\omega$  models (Kolmogorov 1942, Saffman 1970, Wilcox 1988a, 2006). In both models,  $k$  represents the turbulent kinetic energy and is defined by the following equation.

$$k = \frac{1}{2} \left( \overline{u'^2} + \overline{v'^2} + \overline{w'^2} \right) \quad (2.3)$$

For the  $k$ - $\varepsilon$  model,  $\varepsilon$  represents the turbulent kinetic energy dissipation rate within the system. For the  $k$ - $\omega$  model,  $\omega$  represent the ratio of the turbulent kinetic energy dissipation rate to the turbulent kinetic energy,  $k$ . The eddy viscosity for the two-equation models is given by the following.

$$\mu_t = \frac{\rho k}{\omega} \quad k\text{-}\varepsilon \text{ model} \quad (2.4)$$

$$\mu_t = \frac{C_\mu \rho k^2}{\varepsilon} \quad k\text{-}\omega \text{ model} \quad (2.5)$$

where  $C_\mu$  is a constant. Unfortunately, the  $k$ - $\varepsilon$  model fails to adequately predict behavior at walls except under constant-pressure boundary layers and is the only widely used model to suffer from this shortcoming. The  $k$ - $\omega$  model is widely used because of its accurate prediction of turbulent boundary layers with adverse pressure gradients (White 2007).

## 2.10 Advantages of hydraulic modeling

The simplifications and approximations made in the conventional design processes all assume a transport characteristic from the RTD curves. Several investigators stressed the importance of achieving near plug flow conditions. If the hydraulics of the contact tank can therefore be modeled, much of the uncertainty relating to the current design process can be eliminated resulting in the following benefits:

- The operating cost can be reduced due to lower disinfectant dosages
- The probability of forming disinfection and disinfection by products (D/DBP) is reduced.
- The disinfection effectiveness can be improved.

- The capital and operating cost can also be optimized before construction.

## **2.11 CFD Software**

In recent years, the use of numerical models for predicting flows, and transport and dispersion of disinfectants in contact tanks has received considerable attention. Below, a summary of three widely used commercial CFD codes is provided.

### **2.11.1 FLUENT**

Fluent Inc. is a wholly owned subsidiary of ANSYS, Inc., one of the world's leading engineering simulation software developers. Its main product was the computational fluid dynamics (CFD) software named FLUENT.

Fluent is a general-purpose CFD code based on the finite volume method on a collocated grid. FLUENT technology offers a wide array of physical models that can be applied to a wide array of industries.

- **Dynamic and Moving Mesh:** The user simply sets up the initial mesh and prescribes the motion, while FLUENT software automatically changes the mesh to follow the motion prescribed. This is useful for modeling flow conditions in and around moving objects.
- **Turbulence:** A large number of turbulence models are used to approximate the effects of turbulence in a wide array of flow regimes.
- **Acoustics:** The acoustics model lets users perform "on-the-fly" sound calculations.
- **Reacting Flows:** FLUENT technology has the ability to model combustion as well as finite rate chemistry and accurate modeling of surface chemistry.

- Heat Transfer, Phase Change, and Radiation: FLUENT software contains many options for modeling convection, conduction, and radiation.
- Multiphase: It is possible to model several different fluids in a single domain with FLUENT.
- Post-processing: Users can post-process their data in FLUENT software, creating - among other things - contours, pathlines, and vectors to display the data.

The theoretical basis of CFD modeling is the Navier-Stokes fluid dynamics equations, which are used to model fluid parameters such as velocity, temperature, and pressure. FLUENT (ANSYS) is one of most popular CFD software packages that are widely used in engineering research and practice. FLUENT has been successfully used in many previous studies of disinfection contact chambers. In a recent study (Stovin and Saul 1998), the use of the particle tracking routine contained within the FLUENT software for the prediction of sediment deposition in storage chambers is described. The paper details the way in which the particle tracking routine was configured to produce realistic efficiency results for the comparison of storage chamber performance. Consideration was given to the physical characteristics of the sediment, the injection location, the boundary conditions, and a number of relevant simulation parameters. The sensitivity of efficiency prediction to the selection of these parameters is emphasized. The paper also demonstrates the potential application of particle tracking to the prediction of probable deposit locations. In this way, CFD modeling is analogous to conducting a virtual tracer test. Figure 2.2 shows the numerical scheme used to determine RTD-curve in FLUENT.

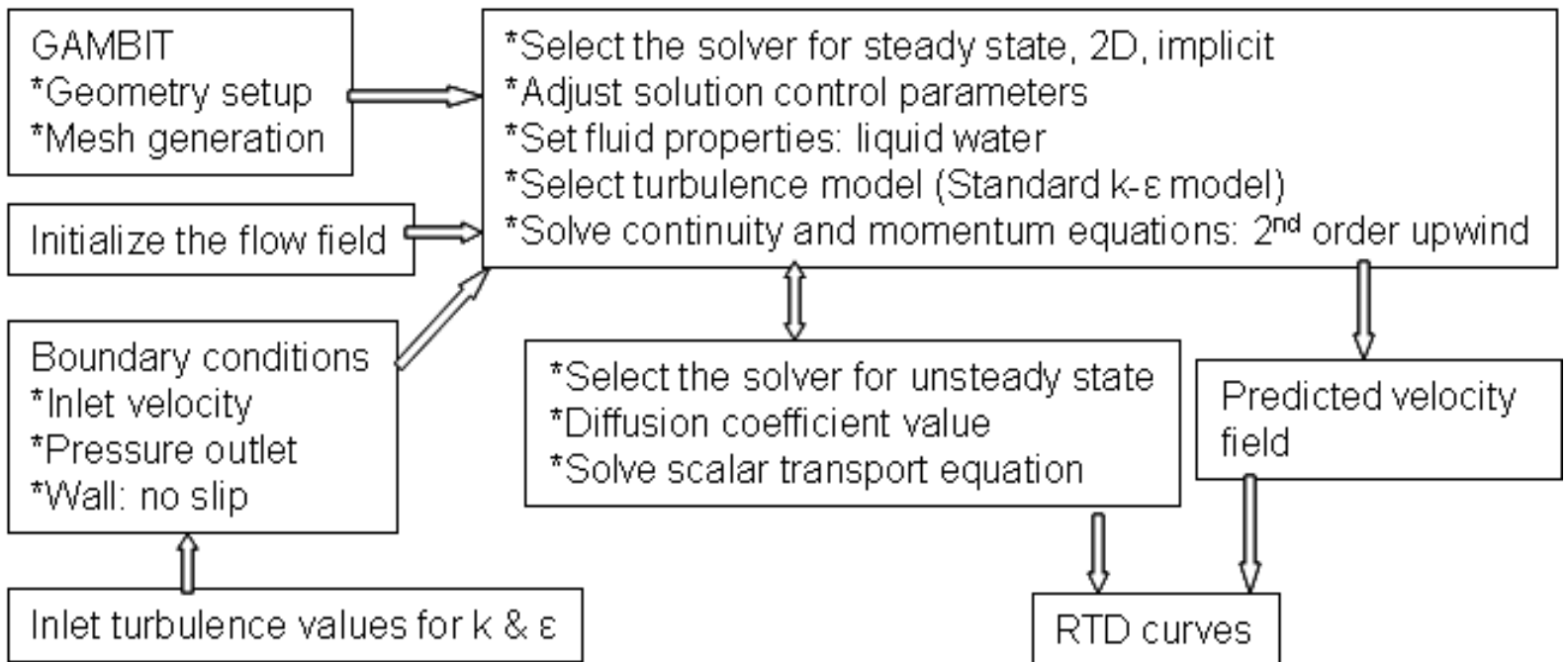


Figure 2.2: Schematic showing the numerical scheme used to determine RTD-curve in FLUENT

### 2.11.2 COMSOL

COMSOL Multiphysics (formerly FEMLAB) is a finite element analysis, solver and simulation software package for various physics and engineering applications, especially coupled phenomena, or multiphysics. COMSOL Multiphysics also offers an extensive interface to MATLAB and its toolboxes for a large variety of programming, preprocessing and postprocessing possibilities. The packages are cross-platform (Windows, Mac, Linux, Unix). In addition to conventional physics-based user-interfaces, COMSOL Multiphysics also allows for entering coupled systems of partial differential equations (PDEs). The PDEs can be entered directly or using the so called weak form (see finite element method for a description of weak formulation).

In Gualtieri's study (Gualtieri 2004), two-dimensional steady-state and time-variable numerical simulations were performed with Multiphysics in contact tank geometry. The paper presents the preliminary results of a numerical study undertaken to investigate hydrodynamics and turbulent transportation and mixing inside a contact tank. Flow field and mass-transport processes are simulated using  $k-\varepsilon$  model and advection-diffusion equation. Numerical results were in good agreement with the observed data for both flow field and tracer transport and mixing. Particularly, numerical results reproduced the recirculation flow regions that were experimentally observed behind the baffles and in the corners at the junctions between the baffles and the tank walls.

### 2.11.3 FLOW-3D

FLOW-3D, computational fluid dynamics software enables highly accurate simulations of free-surface flow using TruVOF, a Volume-of-Fluid technique. In Kim's study (Kim et al. 2008), pilot-scale geometries of disinfection tanks were created using 3-

dimensional computer aided design (CAD) and then transferred to FLOW-3D. The pilot-scale geometries were defined using 3-dimensional FAVOR (fractional area and volume ratios). The FAVOR allows the geometry to be defined exactly, with the mesh of computational cells being mapped onto the boundaries of the geometry. The simulations were used to increase the design efficiency in Korean water treatment plants. Results from FLOW-3D were very similar to results from experimental tracer tests conducted with the pilot-scale tank.

## **2.12 Conclusions**

Though the tracer study described in LTIESWTR is thorough, reliable and traditional, computational fluid dynamics modeling has several advantages over tracer testing. These include:

- Less time spent in modeling compared to full tracer testing
- Does not interrupt plant operations, whereas tracer tests require testing different flow rates and can be involved considerable interruptions to operation
- A range of flow and temperature conditions can be simulated that may not be feasible using physical tracer tests
- Consideration of alternative baffling arrangements that do not physically exist is also possible with CFD modeling
- Further, CFD modeling foregoes the handling of sometimes harmful tracer chemicals (e.g., hydrofluoric acid) and potentially time-consuming process of obtaining regulatory approval to inject tracer into a public water system

Disinfection technology for small water treatment system is the most important element. CFD modeling can successfully predict clearwell residence times for different baffle configurations and flow rates, based on comparisons with full-scale tracer test results. However, it is important to note that before any reliable conclusions are drawn, it is of utmost importance to validate the CFD model that will be used for designing new contact tanks or modifying existing system. In what follows, a validation study of the FLUENT model is carried using an already published tracer and CFD study of an existing water treatment plant.

## **CHAPTER 3**

# **FLOW AND TRACER MODELING IN DISINFECTION TANKS USING COMPUTATIONAL FLUID DYNAMICS**

### **3.1 Introduction**

The flow conditions in existing disinfection contact tanks can be rather complex, with the occurrence of recirculating flow and dead zones, shear and wall generated turbulence, and regions with relatively low flow velocities, such that sophisticated investigative techniques are required to allow detailed assessments of the actual “flow through” characteristics in disinfection contact tanks. Such techniques can involve direct velocity field assessments, e.g. by using laser or acoustic anemometry, and/or by the use of numerical models of the flow and mixing processes in the disinfection tanks. However, the availability of reliable hydrodynamic data for use in the verification of numerical model predictions is limited. Hence, following the literature review, thorough comparisons of the performance of the contact tanks against the predictions of complex two-dimensional CFD codes were performed by following a similar work which had done in a published article (Templeton et al. 2006). This was a convenient choice since tracer studies data were available for validation of the CFD model.

The goal of this chapter is to explain FLUENT and discuss how to model the tracer study in FLUENT using scalar transport equation. In discussing the results, an effort will

be made to explain how CFD can be abused if it is used wrongly. In what follows, a discussion of this validation is presented.

## **3.2 Background**

In the study of Templeton, et al., 2006 (hereafter referred to as Templeton) two-dimensional CFD modeling and full-scale tracer tests (using barium or fluoride) were used to determine the baffle factors of clearwells at three Canadian water treatment facilities (two in Ottawa, Ontario, and one in Peterborough, Ontario). Details of the numerical aspect of this study are outlined below.

### **3.2.1 Numerical Model**

The CFD modeling was performed for each clearwell using Fluent 6.0 and the associated Gambit preprocessor. Two-dimensional models were used because of the large surface area to depth ratio of the clearwells (ratio >180 in all cases) and the previous application of two-dimensional modeling in cases with similar surface area to depth ratios (Hannoun et al. 1998; Crozes et al. 1999). Two-dimensional models drastically reduce the computation time and the overall complexity of the modeling when compared to three-dimensional models. Modeled clearwell geometries were created based on the best available engineering drawings supplied by plant personnel.

### **3.2.2 Geometry**

Geometry creation and grid generation were performed using the Gambit meshing software and then transferred to Fluent for definition of the boundary conditions and solution of the governing fluid dynamics equations. The grids generated in Gambit had

more than 100,000 grid points in each case. The Standard  $k-\varepsilon$  turbulence model and nonslip boundary conditions were specified.

### 3.2.3 Particle tracking

A Fluent 6.0 particle tracking function was used whereby virtual particles (>1000) were released from the same modeled locations as where the actual tracer was injected. The CFD software tracked the residence time of each particle, from which  $T_{10}$  values and baffle factors were calculated. The CFD models can allow tracers to be considered as a chemical species, however in this case particle tracking was used so that the paths of discrete microorganisms through the clearwells could be modeled, since it is the residence time of pathogenic organisms that is of primary interest in disinfection. The particles were assumed to be spherical and of approximately the same density as the water.

### 3.2.4 Results

The results of this study suggest that CFD modeling can successfully predict clearwell residence times for arrange of baffle configurations and flow rates, based on comparisons with full-scale tracer test results. The two-dimensional models developed in this study provided baffle factor estimates that matched tracer results to within 17% in all cases, and were accurate to within 10% in most cases (Templeton et al. 2006). Model prediction effectiveness was related to flow rate, clearwell volume, or clearwell baffle configuration for the examples that were evaluated.

### 3.3 Problem statement

At the Britannia Water Purification Plant (WPP) (Ottawa, Ont.), there are two clearwells with different serpentine baffling configurations, referenced to as clearwell I and clearwell II. Figure 3.1 shows the normalized barium concentration profile in Templeton's paper for the Britannia WPP (Ottawa, Ont.) clearwell I effluent sampling location.

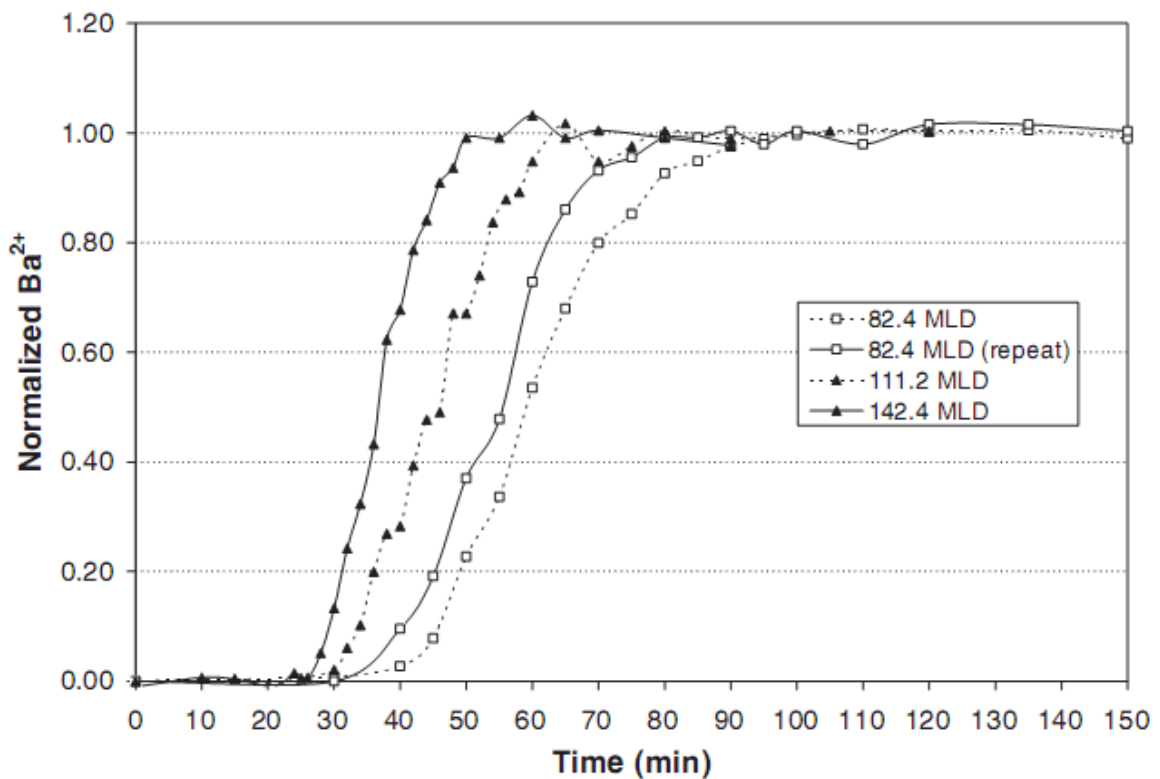


Figure 3.1: the normalized barium concentration profile in Templeton's paper for the Britannia WPP (Ottawa, Ont.) clearwell I effluent sampling location.

Clearwell I has volume of  $4530 \text{ m}^3$ . It is between 87% and 93% full during the tracer testing. From Figure 3.1, the flow rates through clearwell I for the tracer tests and modeling were 82.4, 111.2, and 142.4 million liters per day (MLD). The test at 82.4 MLD was repeated to demonstrate the reproducibility of the test results. The two

replicate tracer responses had almost identical profiles but were shifted by approximately 5 minutes due to experimental errors.

In what follows, a discussion of the CFD study that was carried out to compare with both the tracer study results and the CFD model results of Templeton is provided. For this purpose, a study of the clearwell I (Templeton et al. 2006) at a flow rate of 82.6 MLD was done. The main aim of doing this work is to provide an overview of the problem set-up process in CFD and validate the model using the experimental data in Figure 3.1.

### 3.4 Numerical solutions and results in FLUENT

The computational fluid dynamics software FLUENT, version 12.0, developed by Fluent/ANSYS was employed to perform highly resolved two-dimensional (planar) simulations in the domain shown in Figure 3.2.

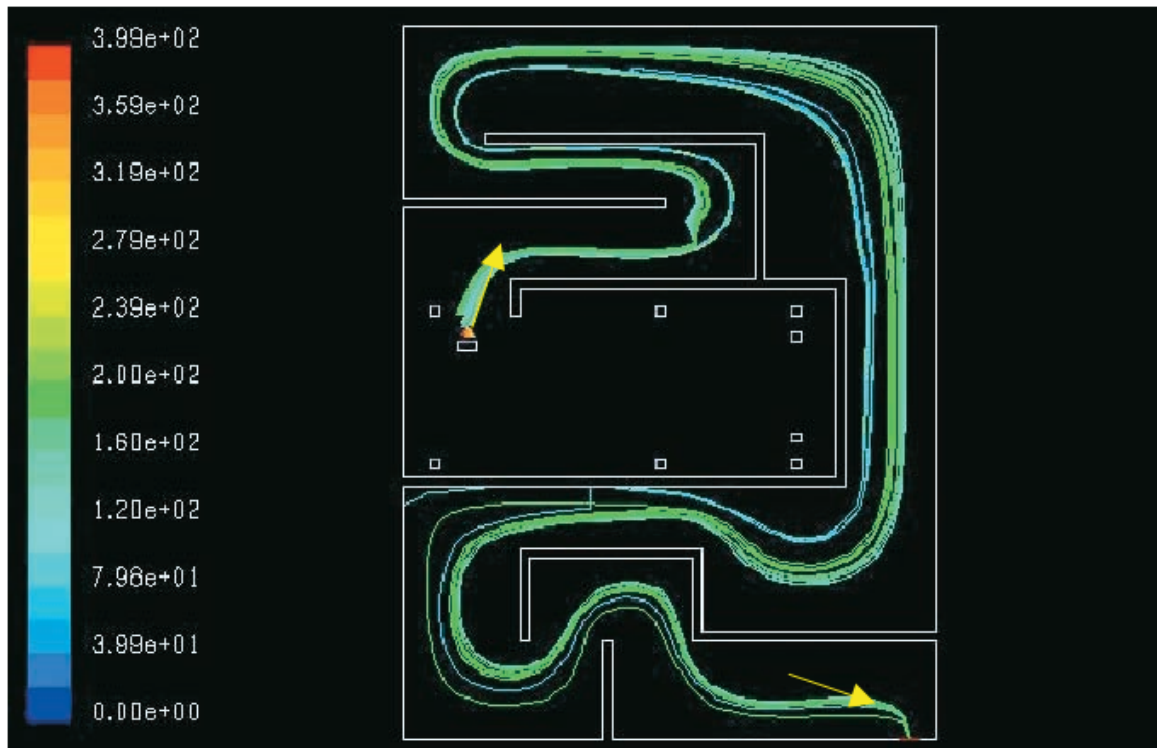


Figure 3.2: Example particle tracks through Britannia WPP (Ottawa, Ont.) clearwell I at 111.2 MLD. Arrows show the direction of flow in and out. (Templeton et al. 2006)

### 3.4.1 Geometry development

FLUENT is a finite-volume code that solves the Navier-Stokes equations and allows the use of structured or unstructured meshes. Here, we use this code to solve the Reynolds-Averaged Navier-Stokes (RANS) and scalar transport equations on an unstructured triangular mesh as shown in Figure 3.3.

A grid independence study was carried out to determine the level of convergence and selection of an optimal mesh that will yield accurate results with affordable computational costs. Table 3.1 and Figure 3.3 show the results of the grid independence study (using the domain for clearwell II on Templeton's work). Four different count sizes of the grid are chosen, which are: 0.1, 0.5, 0.25 and 0.125, respectively.

**Table 3.1: Grid independence study on Clearwell II.**

Grid	Count Size	Mesh Face	No. of Cells	Maximum Velocity (m/s)	$\Delta(V_{\max})$
1	1.000	2188	15048	1.27	
2	0.500	7948	54663	1.61	0.34
3	0.250	30946	212833	1.64	0.03
4	0.125	123699	850747	1.65	0.01

Figure 3.3 shows the convergence of the velocity simulations with different mesh faces inside the domain (see also Figure 3.4). Based on the convergence results, a mesh with a count size of 0.25 was chosen as the optimal mesh for this study. The shape of the cells used in the mesh can be either square shaped or triangular. Two simulations were carried and the results are shown in Figure 3.5. It is clear that the triangular meshes work better here in this case since it allows for better grid refinement in regions where rapid changes in velocities are expected (for example around baffle corners). The final grid used for this study is shown in Figure 3.6.

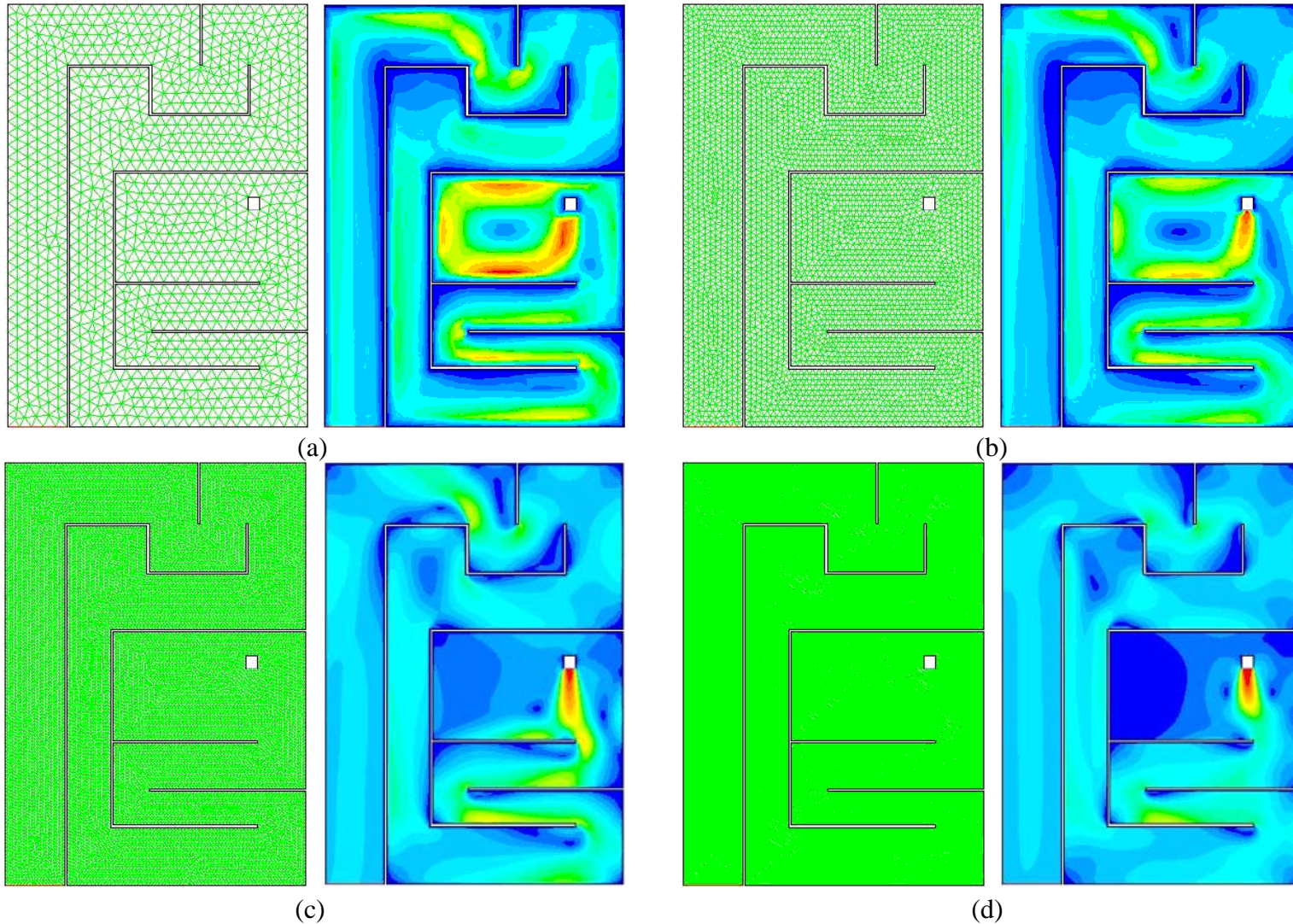


Figure 3.3: Number of mesh faces inside the grid versus the maximum velocity of the simulations for the clearwell II.  
 (a) Mesh faces = 2188, (b) Mesh faces = 7948, (c) Mesh faces = 30946 and (d) Mesh faces = 123699

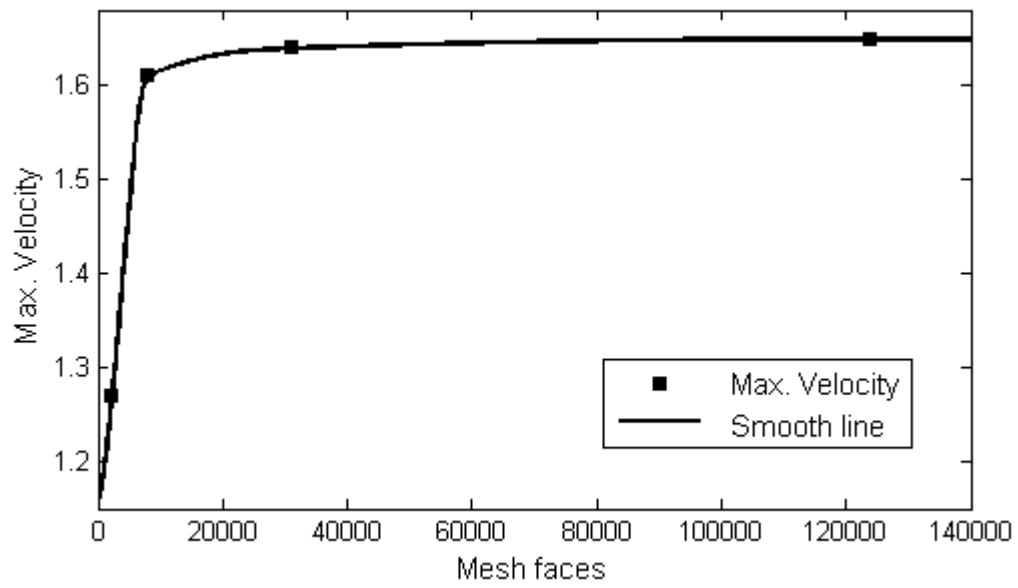


Figure 3.4: Grid independence study of clearwell II.

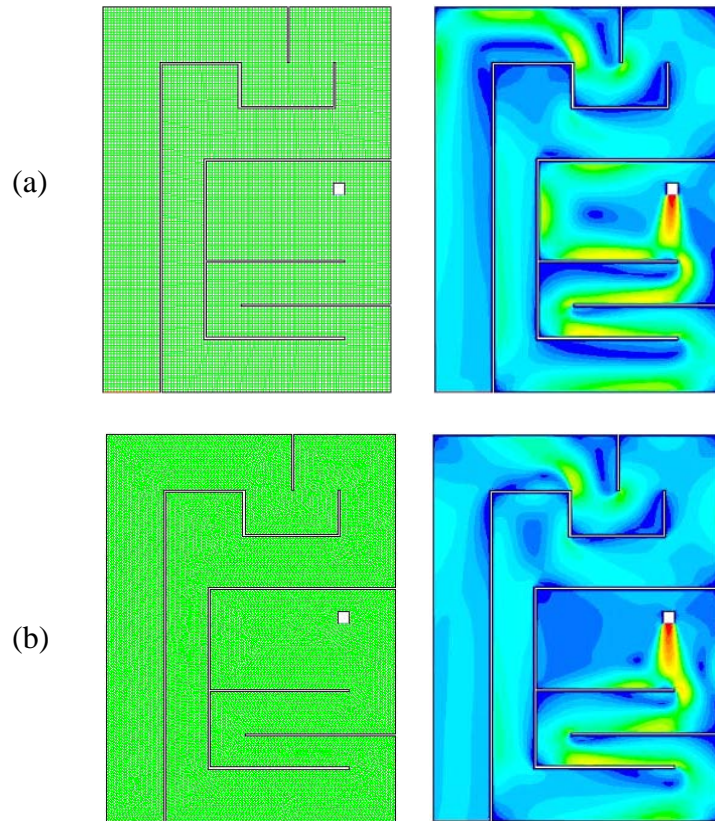


Figure 3.5: Shape of cells inside the grid versus the maximum velocity of the simulations:  
 (a) Square cells, (b) Triangular cells.

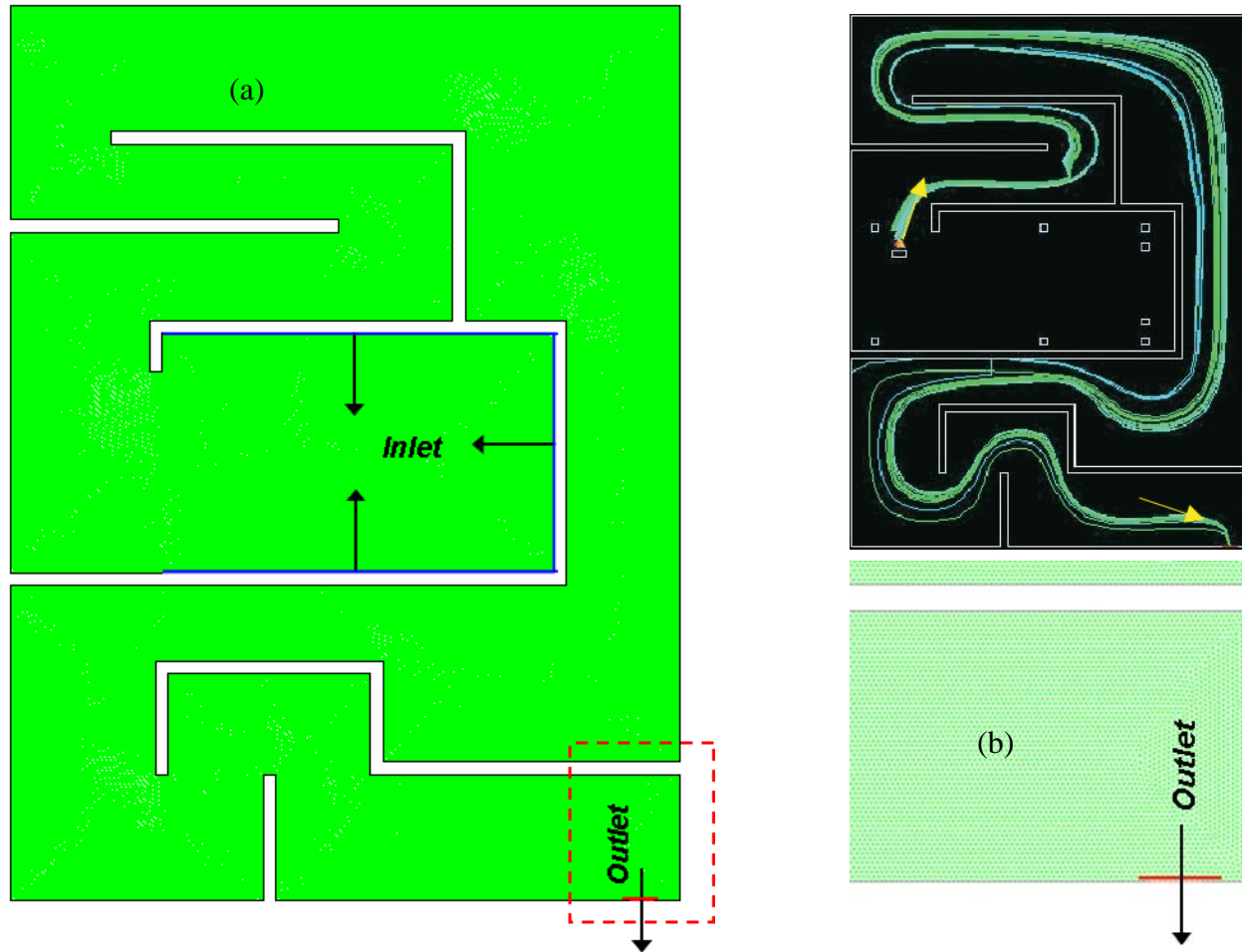


Figure 3.6: (a) The unstructured computational mesh for clearwell I in Britannia WPP (Ottawa, Ont.);  
(b) Zoomed view of the mesh near the clearwell outlet area.

The computational mesh shown in Figure 3.6 is determined to yield converged results for the clearwell II configuration which has 30946 mesh faces, approximately equal to 212833 cells.

### 3.4.2 Velocity field

The standard  $k$ - $\varepsilon$  model (Launder and Spalding 1974) was chosen for the turbulence closure with standard empirical coefficients. The simulations are firstly performed to get the velocity field in the tank.

The steady state turbulent velocity field is calculated using the RANS equations with a second-order upwind scheme. No-slip boundary conditions were imposed on all walls and baffles. Constant volume flow rate, kinetic energy  $k$  and kinetic energy dissipation rate  $\varepsilon$  were specified at the inlet, while the outlet was treated as a pressure outflow discharging to the atmosphere.

The velocity fields show the presence of stagnant (dead zone) close to the baffles due to flow separation which impedes uniform mixing of the tracer (See Figure 3.7). To better show the solution of the model, the simulated pathline contour is shown in Figure 3.7(b).

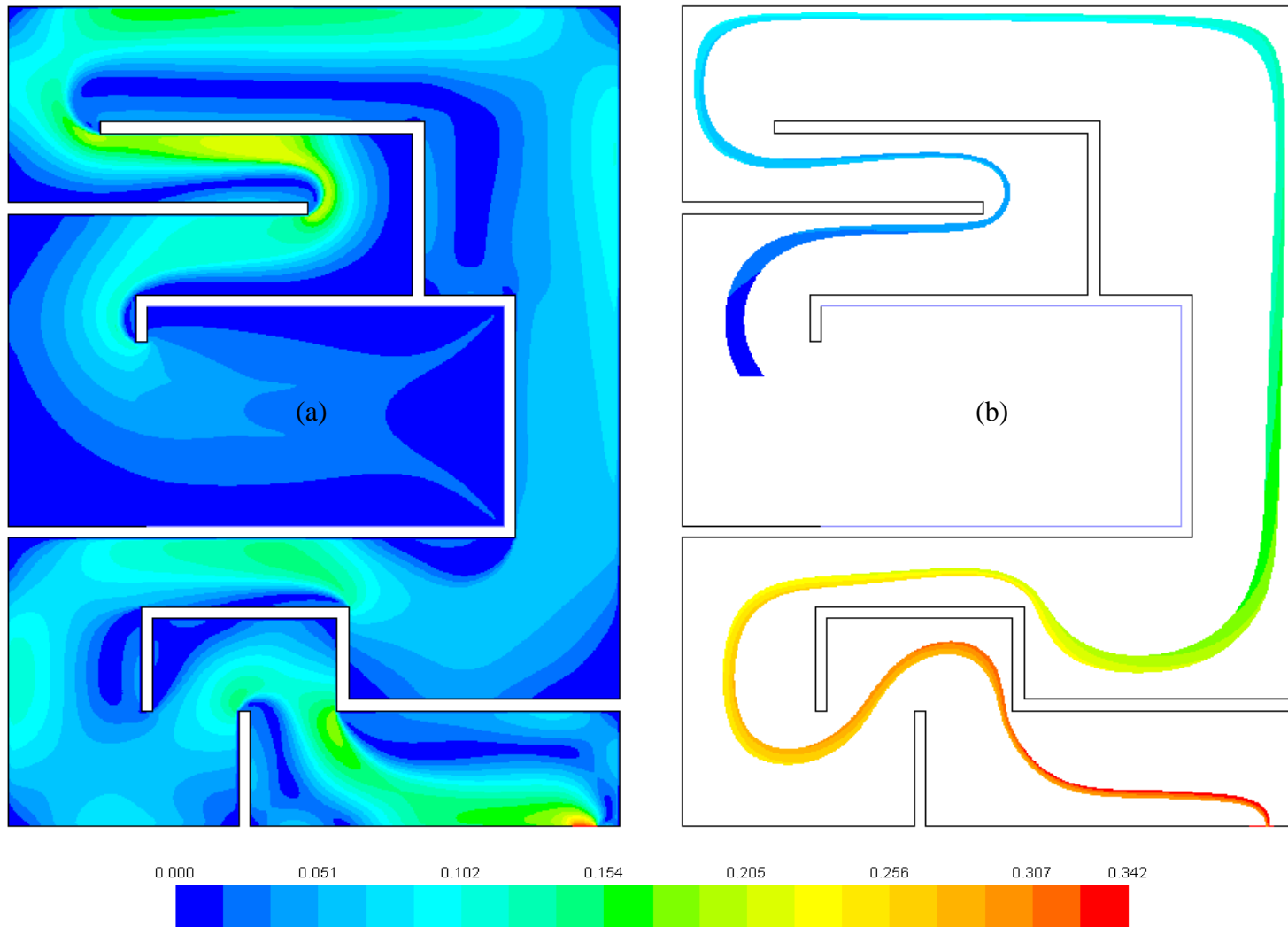


Figure 3.7: (a) Simulated Steady-state planar velocity field (color bar unit: m/s) in clearwell I of Britannia WPP (Ottawa, Ont.); (b) Simulated steady-state pathline contour in clearwell I (the color represented the travel time).

### 3.4.3 Scalar transport

With the predicted steady state velocity field from the first step, the tracer concentration is calculated using the advection-diffusion equation given by

$$\frac{DC}{Dt} = \frac{\partial C}{\partial t} + \bar{U} \cdot \nabla C = \nabla \cdot \left( \left( \kappa + \frac{\nu_t}{Sc_t} \right) \nabla C \right) \quad (3.1)$$

where  $C$  is the tracer concentration (e.g. chlorine),  $\bar{U}$  is the steady state turbulent velocity field,  $\kappa$  is the molecular diffusivity of the tracer,  $\nu_t$  is the turbulent eddy viscosity and  $Sc_t$  is the turbulent Schmidt number. Both  $\bar{U}$  and  $\nu_t$  are obtained from the steady state solution of the momentum equations from the first step. The turbulent Schmidt number  $Sc_t$  is given as 0.7, a value widely accepted to be appropriate for neutrally stratified flow conditions (for a justification see e.g. Venayagamoorthy and Stretch 2010). For details on how the turbulent diffusivity ( $\nu_t/Sc_t$ ) is obtained is given in Appendix B.

Figure 3.8 shows how the scalar concentrations inside the clearwell I in time. The scalar concentrations are shown in intervals of 500 seconds. Dispersion as the flow turns and separates around the baffles is evident.

Other models for determining the residence distribution are available for the dispersion of particles in the domain, such as the particle tracking function in FLUENT for virtual particles (Templeton et al. 2006) and the discrete phase models (Meroney 2008).

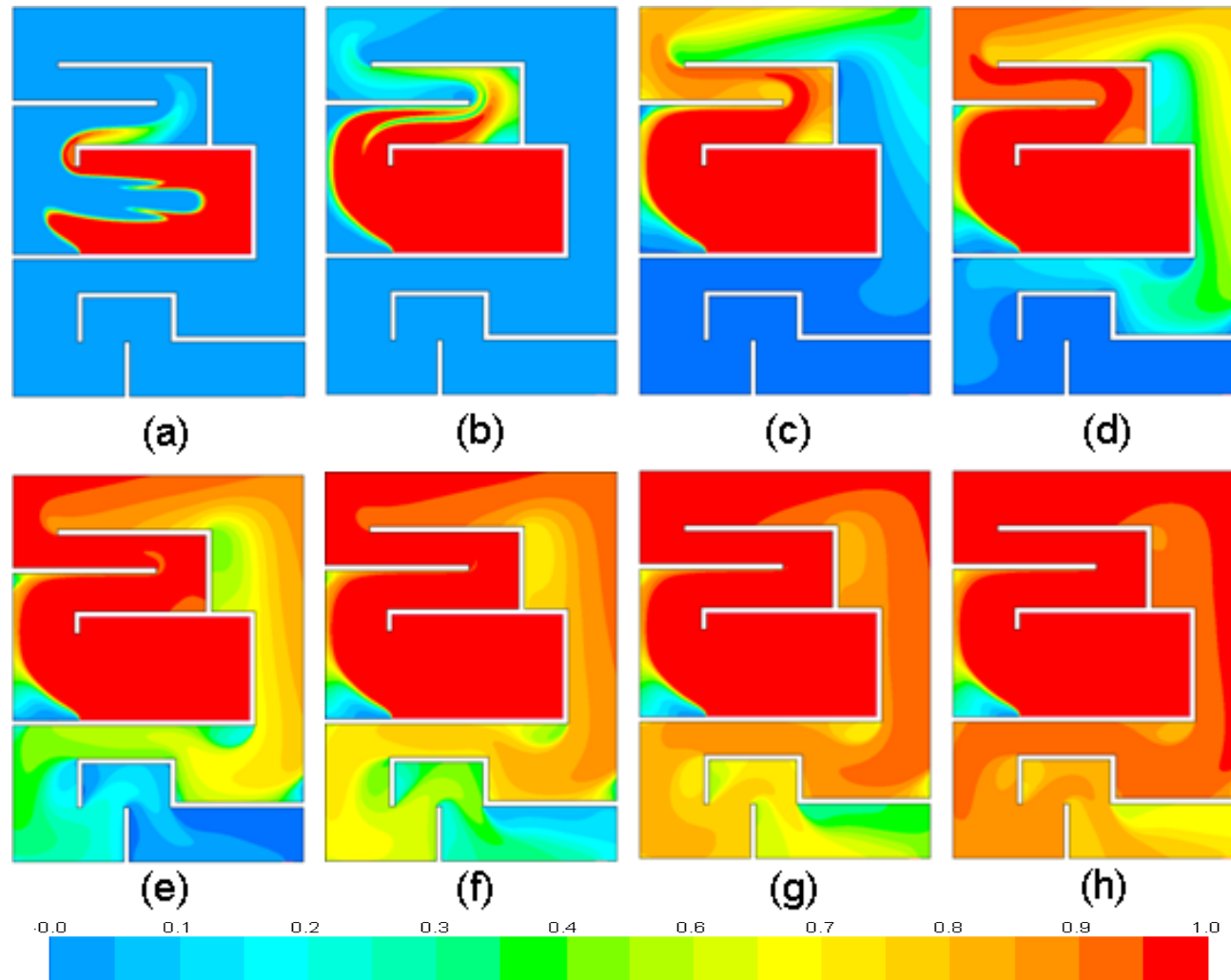
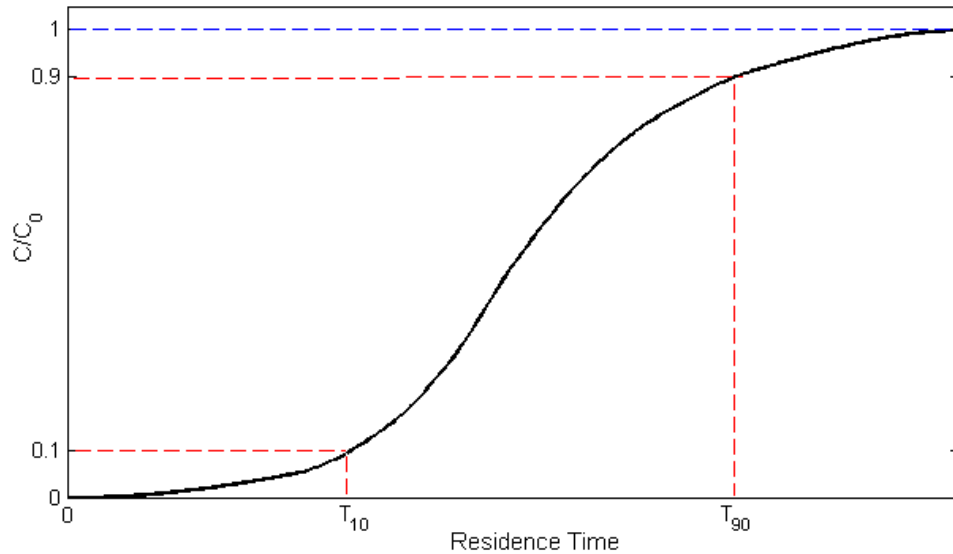


Figure 3.8: Time sequence showing the scalar concentration in clearwell I introduced as a step dosage: (a) Flow time = 500s, (b) Flow time = 1000s, (c) Flow time = 1500s, (d) Flow time = 2000s, (e) Flow time = 2500s, (f) Flow time = 3000s, (g) Flow time = 3500s and (h) Flow time = 4000s. The color bar gives the magnitude of the normalized scalar concentration.

### 3.4.4 Validation of CFD models

Solutions of equation (3.1) can be used to obtain the RTD curve at the outlet of the tank corresponding to a step tracer input at the inlet where the concentration is set as  $C_0 = C_{max} = 1$ . The value of the scalar is monitored at the outlet as a flux. The variation of concentration-time draws the RTD curve of a step dosage tracer study as shown in Figure 3.9. In a RTD curve,  $T_{10}$  is the residence time when  $C/C_0$  reaches 0.1, and  $T_{90}$  is the time when  $C/C_0$  passed the value of 0.9. Mathematically, mean residence time  $T_m$  of a tank can be provided by equation (3.2).

$$T_m = \frac{1}{C_{max}} \int_0^{C_{max}} t dC \quad (3.2)$$



**Figure 3.9: RTD curve at the outlet when the tracer is injected as a step dosage.**

Figure 3.10 shows the results from the CFD simulations, which shows a good agreement with the experiment data from Templeton's study. The baffle factor from

tracer study when flow rate is 82.4 MLD is 0.64 as shown in Templeton's study. From Figure 3.1, it is straight forward to see that  $T_{10}$  is around 45 minutes for the curve of flow rate equal to 82.4 MLD. Thus, it is easy to show the volume of clearwell I was 4188 m<sup>3</sup> when the tracer studies were conducted indicating that the tank was 90% full. Baffle factor from our CFD simulation is also around 0.64.

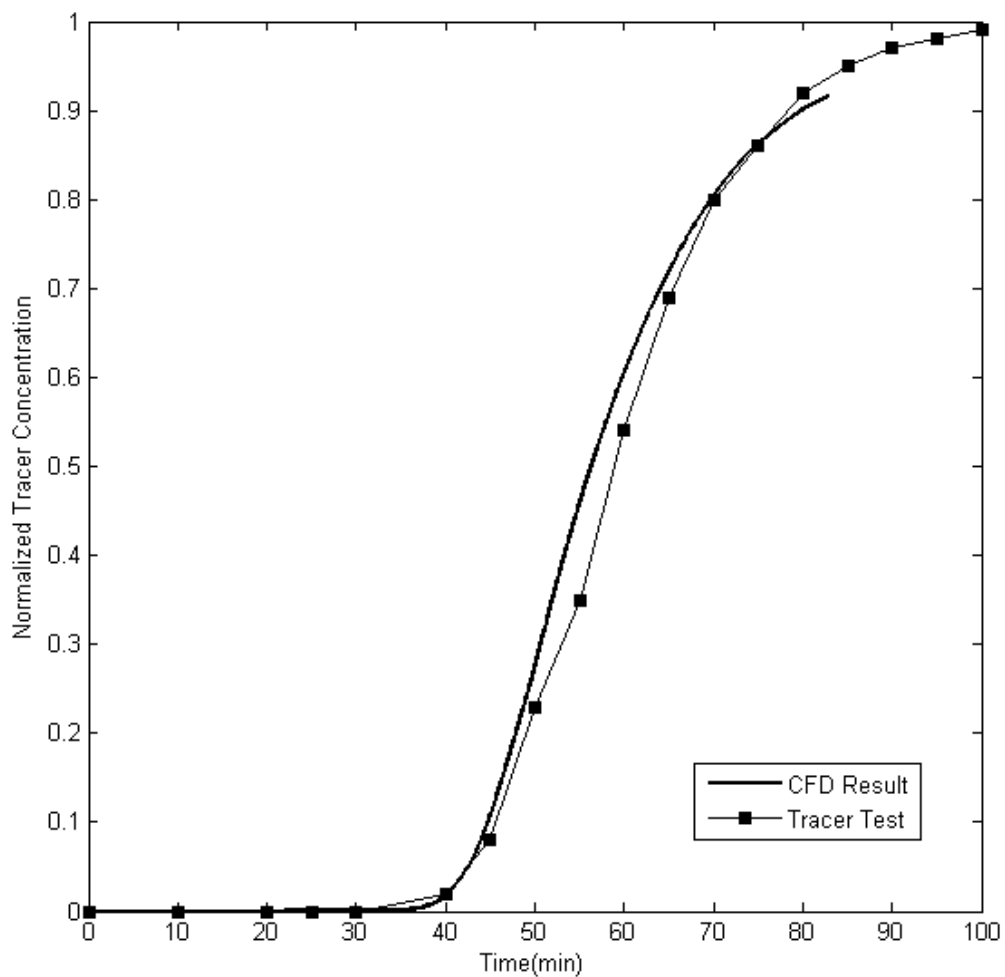


Figure 3.10: CFD results validation.

### **3.5 Comparison of particle tracking and pathlines**

In Templeton's study, the differences between their CFD results and experiment data are much larger. They explain the small differences as slightly deceptive due to the limited range of the baffle factors that were considered in the study (i.e., baffle factor = 0.6–0.8). For example, simply guessing an average baffle factor (say 0.7) for all cases would have produced small errors comparable to those from using the sophisticated CFD model.

After further look at their simulation results, it became evident that they did not model the mixing between fluid particles since they used pathlines to determine the baffle factor. However, they do not show the RTD curves from their CFD studies. A reason for not showing the CFD results against the tracer study results (e.g. Figure 3.10 in this study) is the lack of a good agreement between experimental and CFD results which is mainly to due to the absence of key physics for describing mixing in their model. If the tank itself has a better hydraulic efficiency, the differences between simulations with and without considering mixing will be smaller, i.e. for near plug flow contact tanks.

### **3.6 Summary**

In this chapter, results from highly resolved two-dimensional CFD simulations of turbulent mixing and transport of a passive tracer in a model tank has been presented. By comparing CFD results of Templeton et al. (2006) CFD studies and the present CFD study, the importance of correctly modeling the physics of a process such as mixing in CFD is highlighted

In this study, the CFD model provided information that would not be otherwise known, such as the existence and location of dead zones in sections of the tank. This study also vindicates the use of CFD as an important design tool to limit the number and extent of tracer studies. However, this study also shows that the importance of validating a CFD model using a tracer study.

## **CHAPTER 4**

### **HYDRAULIC EFFICIENCY OF BAFFLED DISINFECTION TANKS**

#### **4.1 Introduction**

This chapter is essentially a modified version of a peer-reviewed conference article that will be presented at the Sixth International Symposium on Environmental Hydraulics (ISEH) in June 2010 in Athens, Greece. A condensed version of this chapter is currently under preparation for submission to the ASCE Journal of Environmental Engineering.

The goal of this chapter focuses on understanding the internal hydraulic efficiency of baffled disinfection contact tanks. In this chapter, the footprint of the laboratory scale disinfection tank used by Shiono and Teixeira (2000) in their experimental studies is used to quantify the hydraulic efficiency of the tank as a function of the number of baffles.

#### **4.2 Problem statement**

Figure 4.1 shows the footprint of the tank we employ in this study which represents the main aspects of the seven baffle tank configuration used by Shiono and Teixeira (2000) in their experimental studies (see also Shiono et al. 1991). The tank is 1.995-m-long, 0.94-m-wide, and 0.6-m-deep. It represents a 1:8 scale model of the Embsay Chlorine Contact Tank located in West Yorkshire, England. Tracer studies were conducted by Shiono et al. (1991) with a continuous discharge of  $1.17 \times 10^{-3}$  m<sup>3</sup>/s entering

the tank, resulting in a mean water depth of 0.536 m and an initial mean cross-sectional velocity of 0.0104 m/s at the inlet, based on a uniform inlet width of 0.21 m. In this study, we examine the effect of number of baffles on the internal hydraulics and disinfection contact times by varying the number of baffles in the tank from 0 to 10. The same volume flow rate is used for all the simulations, which is equal to the value used in the experiments of Shiono et al. (1991).

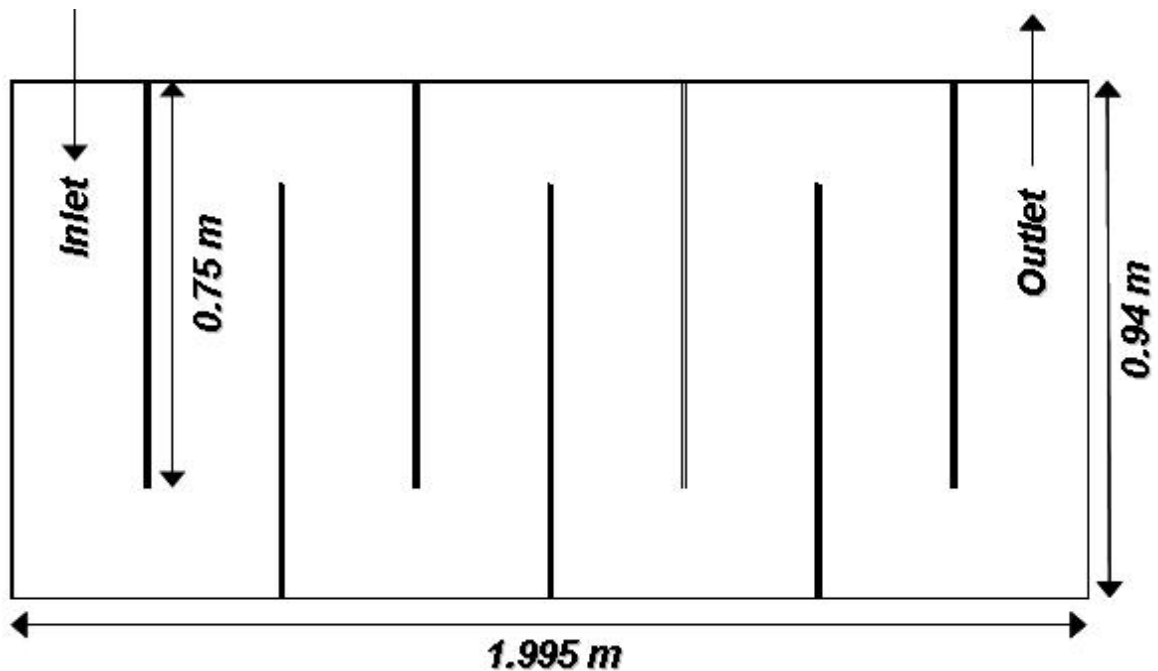


Figure 4.1: Schematic showing the footprint of the contact tank with 7 baffles used in the simulations for this study.

### 4.3 Numerical framework

We employ the CFD software FLUENT, version 12.0, developed by Fluent/ANSYS to perform highly resolved two-dimensional (planar) simulations in the domain shown in Figure 4.1.

A grid independence study was carried out to determine the level of convergence and selection of an optimal mesh that will yield accurate results with affordable computational costs. Table 4.1 and Figure 4.2 show the independence study in detail. Four different interval sizes of the grid are chosen, which are: 0.1, 0.02, 0.01 and 0.005, respectively. By comparing the maximum velocity with the interval size of the grid (see Figure 4.2), an interval size of 0.02 provides the optimal choice in terms of convergence and computational costs.

**Table 4.1: Grid independence study on 7 baffles tank.**

Grid	Interval Size	Total Cells	Max. Velocity	$d(V_{\max})$
1	0.100	514	0.0163	
2	0.020	9474	0.0217	0.0054
3	0.010	37393	0.0232	0.0015
4	0.005	147240	0.0226	0.0006

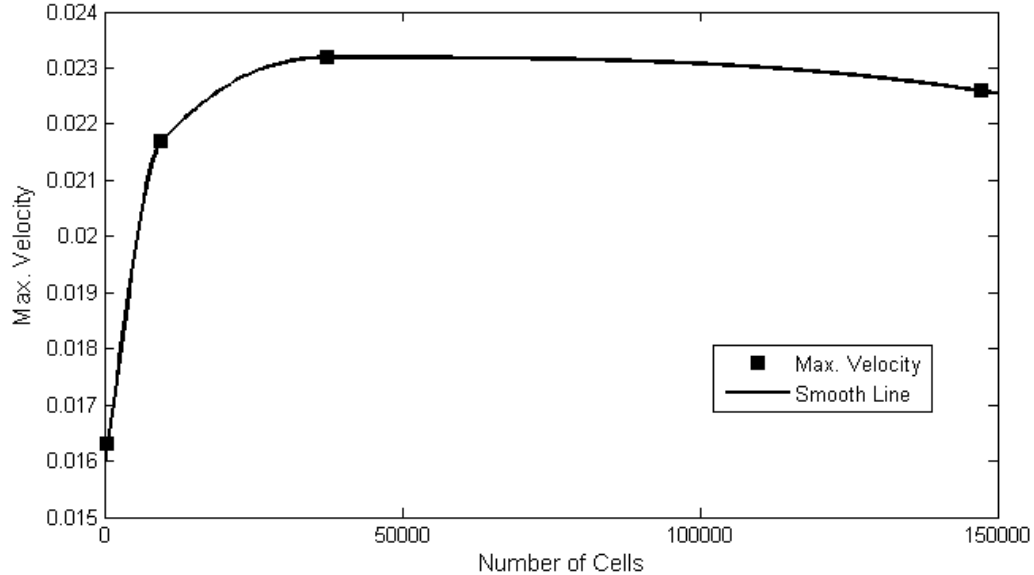
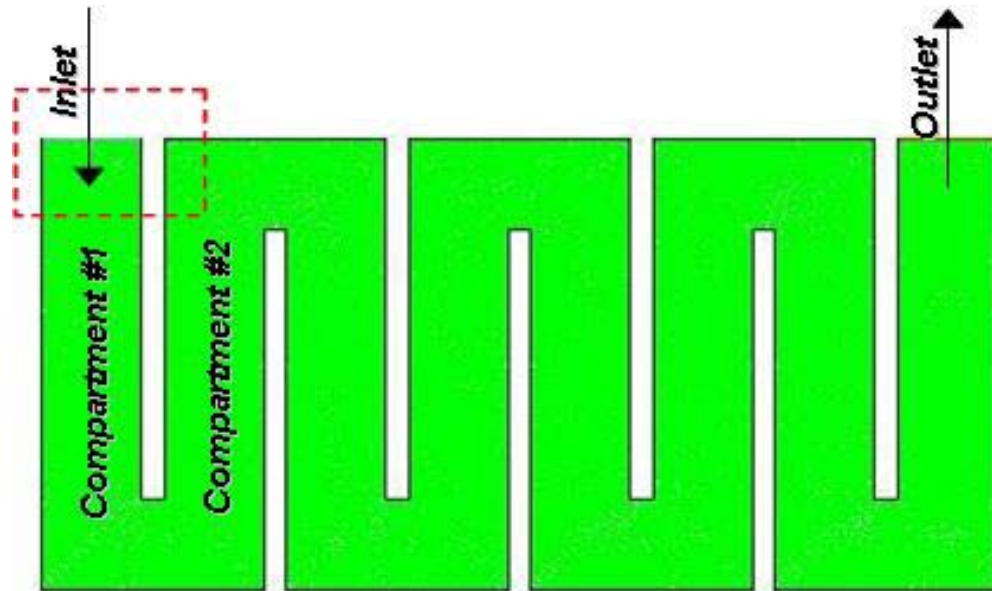


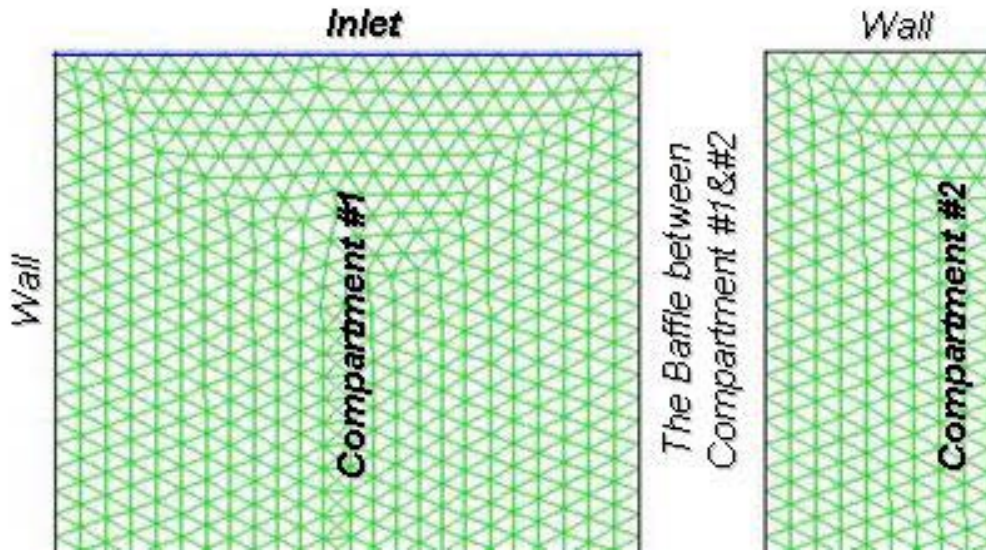
**Figure 4.2: Number of cells inside the grid versus the maximum velocity of the simulations.**

The computational mesh shown in Figure 4.3 is determined to yield converged results for the seven baffle configuration and has approximately 37,500 cells. Similar number of

volumes cells are used for the 10 other baffled configurations that are simulated for this study.



(a)



(b)

Figure 4.3: (a) The unstructured computational mesh for the seven-baffled contact tank; (b) Zoomed view of the mesh near the tank inlet area.

The simulations are performed in two steps. First, the steady state turbulent velocity field is calculated using the RANS equations (see Appendix B for more details) with a

second-order upwind scheme. No-slip boundary conditions were imposed on all walls and baffles. Constant volume flow rate, kinetic energy  $k$  and kinetic energy dissipation rate  $\varepsilon$  were specified at the inlet, while the outlet was treated as a pressure outflow discharging to the atmosphere. Second, with the predicted steady state velocity field from the first step, the tracer concentration is calculated using the advection-diffusion equation given by equation (3.1) given in Chapter 3. Solutions of equation (3.1) can be used to obtain the RTD curve at the outlet of the tank.

#### **4.4 Results and discussions**

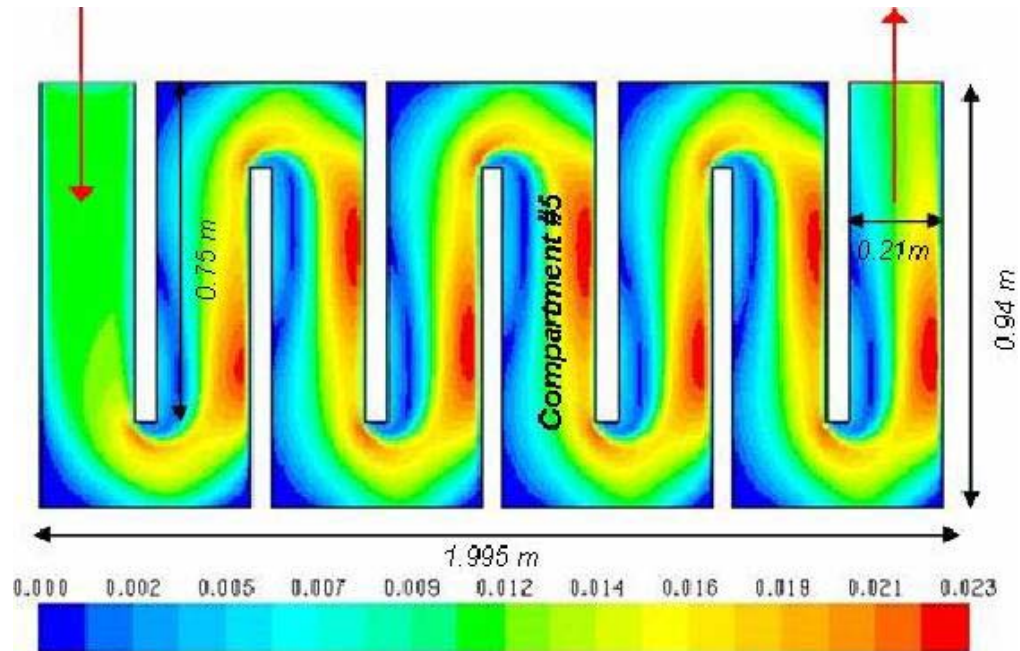
We carried out a total of 11 simulations for this study representing tanks with 0 to 10 baffles. In this section, validation results for the seven baffle tank configuration are presented first. Following which, discussion on the effect of baffle numbers on baffle factors is provided. The effect of dead zones on the hydraulic efficiency is then quantified. In the end, an extensive analysis on baffle factors for a given footprint of a tank with variation of volume flow rates at the inlet is shown.

##### **4.4.1 The comparison of measured and modeled velocity distributions**

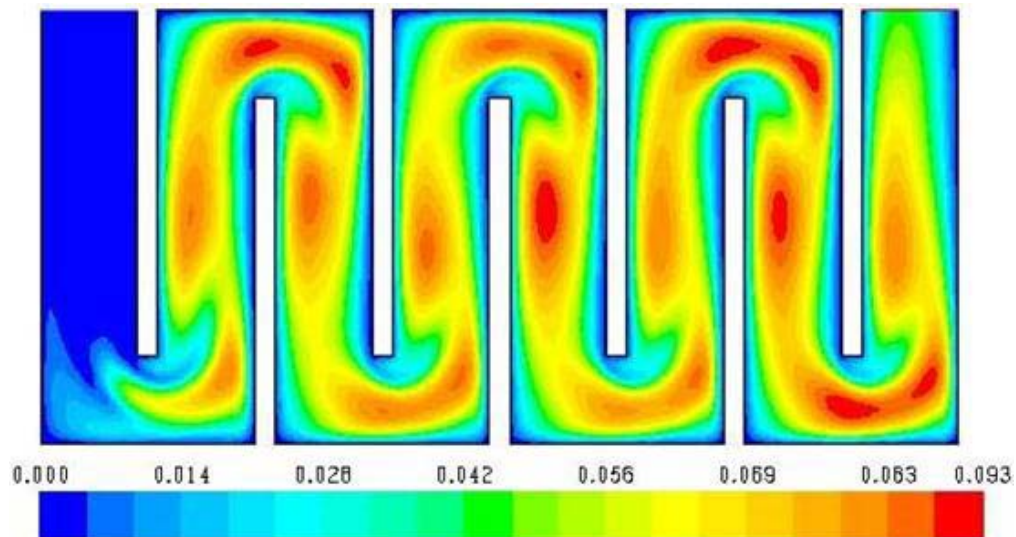
Figure 4.4 shows the steady-state planar velocity and turbulent dynamic eddy viscosity distribution in the tank for the seven baffle configuration shown in Figure 4.1. The velocity distribution highlights the flow patterns such as dead zones that occur in the tank due to separation as shown in Figure 4.4(a).

In an effort to validate the CFD model, we used the experimental data for the longitudinal velocity field that was available across a section in compartment 5 of the tank from the experiments of Shiono et al. (1991). Figure 4.5 shows good agreement

between the simulated longitudinal velocity across a section in compartment 5 of the tank and the experimental results indicating the adequacy of the numerical approach used to resolve the flow field.



(a)



(b)

Figure 4.4: Simulated turbulent flow properties in the seven-baffled tank depicted in Figure 4.1; (a) Steady-state planar velocity field (color bar unit: m/s) and (b) turbulent dynamic eddy viscosity (color bar units: Pa·s), respectively.

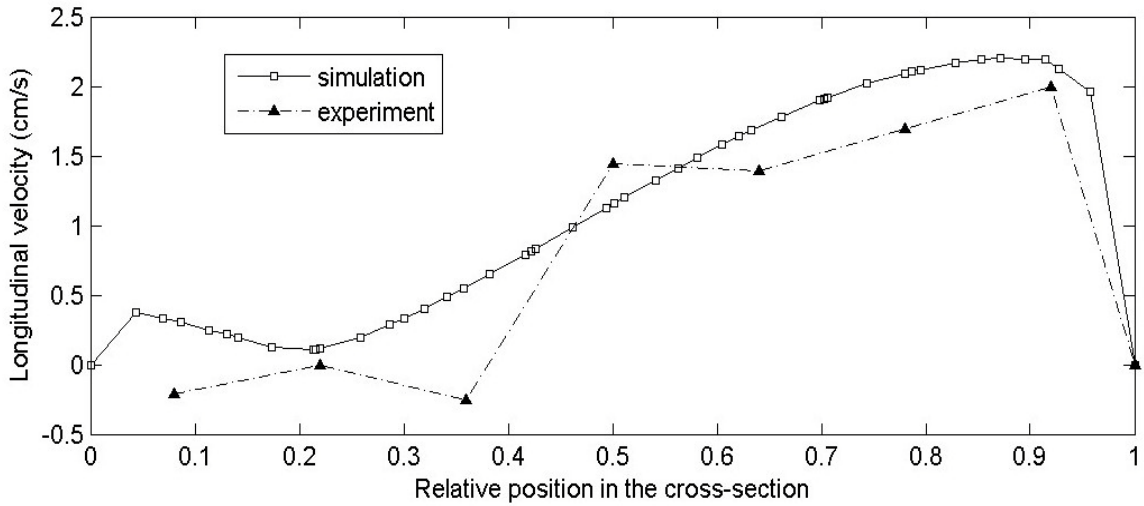


**Figure 4.5: Comparison of computed longitudinal velocity with experimental velocity data along a cross-section in compartment 5 shown in Figure 4.4(a).**

#### 4.4.2 Simulation of scalar transport in FLUENT

The time sequence of the transport of a passive scalar inside the seven-baffle tank is shown in Figure 4.6. We recorded the scalar contours every 100 seconds during the whole flowing simulation. These results indicate that the flow becomes dispersive due the turbulence induced in the flow as a result of separation that occurs around baffles. This is evident even from the velocity field shown in Figure 4.4 (a).

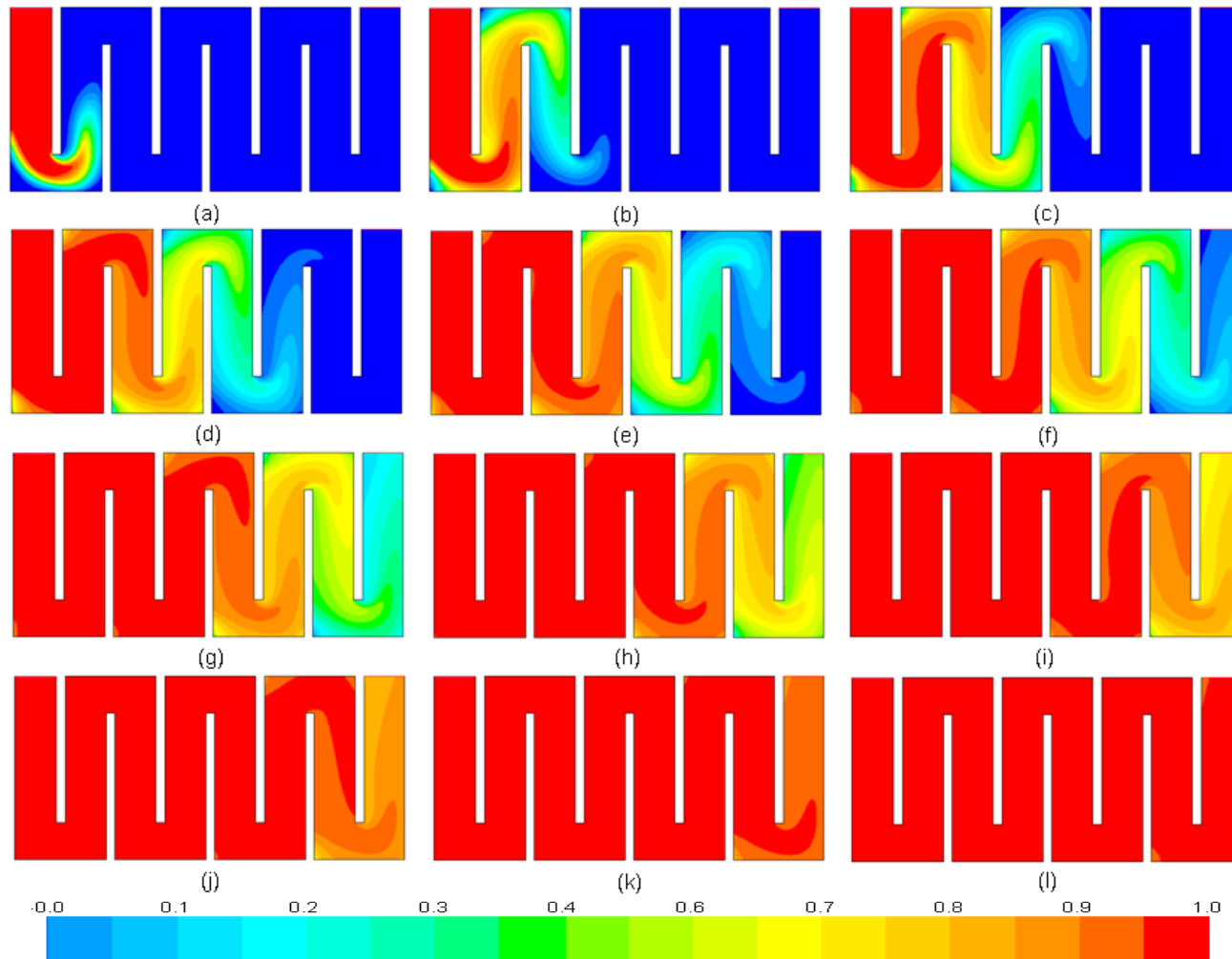


**Figure 4.6: Scalar concentrations in the 7-baffles tank as a step dosage:**

(a) Flow time = 100s, (b) Flow time = 200s, (c) Flow time = 300s, (d) Flow time = 400s, (e) Flow time = 500s, (f) Flow time = 600s, (g) Flow time = 700s, (h) Flow time = 800s, (i) Flow time = 900s, (j) Flow time = 1000s, (k) Flow time = 1100s and (l) Flow time = 4000s. The color bar gives the magnitude of the normalized scalar concentration

Using the scalar transport equation (equation (3.1)), the RTD curve of seven-baffle tank is obtained (see Figure 4.7). The  $T_{10}$  and  $T_{90}$  values for this seven-baffle tank can be obtained either from the RTD curve or from a report file of the flow time and scalar values at the outlet from FLUENT. For this seven-baffle tank,  $T_{10}$  is equal to 617 s and  $T_{90}$  is 1080s. The scalar contours inside the tank is recorded when we are doing the simulation. In Figure 4.8, the scalar contours at  $T_{10}$  and  $T_{90}$  are shown.

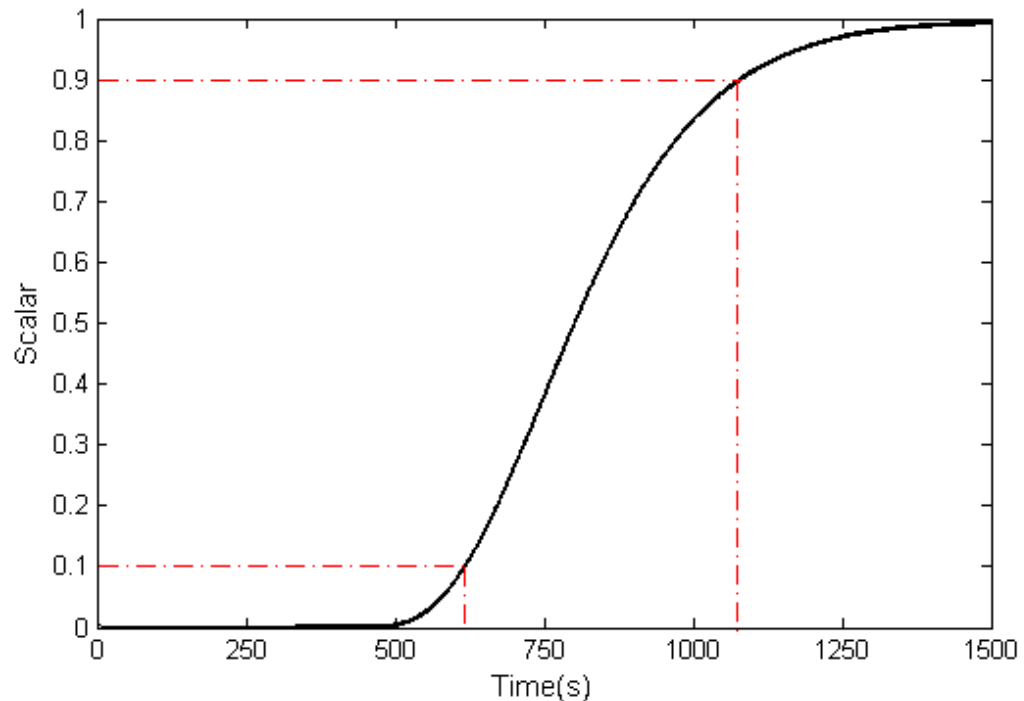


**Figure 4.7: Simulated RTD curve of tracer at the outlet for the seven baffle tank shown in Figure 4.1 for a step trace input at the inlet.**

#### 4.4.3 The effect of the baffle numbers on baffle factors

The seven baffled tank's initial geometry that is shown in Figure 4.1 was modified by changing number of baffles from 0 to 10 while maintaining the same footprint. Figure 4.9 shows the variations in the velocity field for all the eleven different numbers of

baffles. Figure 4.9(a) shows an unbaffled tank where the flow clearly short circuits and results in poor baffling condition with a baffle factor close to 0.2, comparing with Table 1. The flow patterns become more streamlined as the number of baffles increase as expected allowing for better baffling condition (see Figure 4.9(b)-(k)).

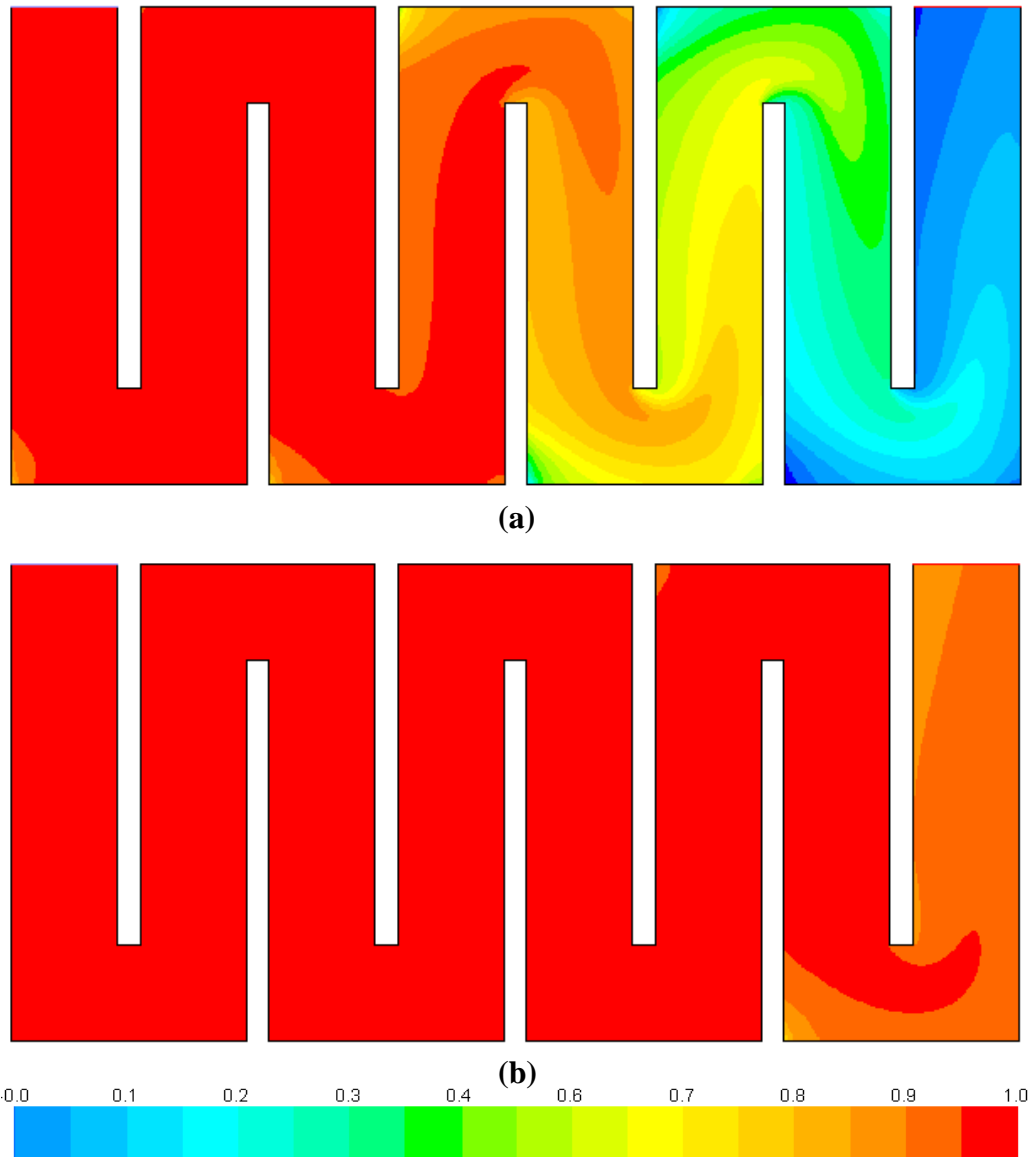


Figure 4.8: Scalar contours at  $T_{10}$  and  $T_{90}$  in the seven-baffle tank as a step dosage: (a) Flow time =  $T_{10} = 617$ s and (b) Flow time =  $T_{90} = 1080$ s. The color bar gives the magnitude of the normalized scalar concentration.

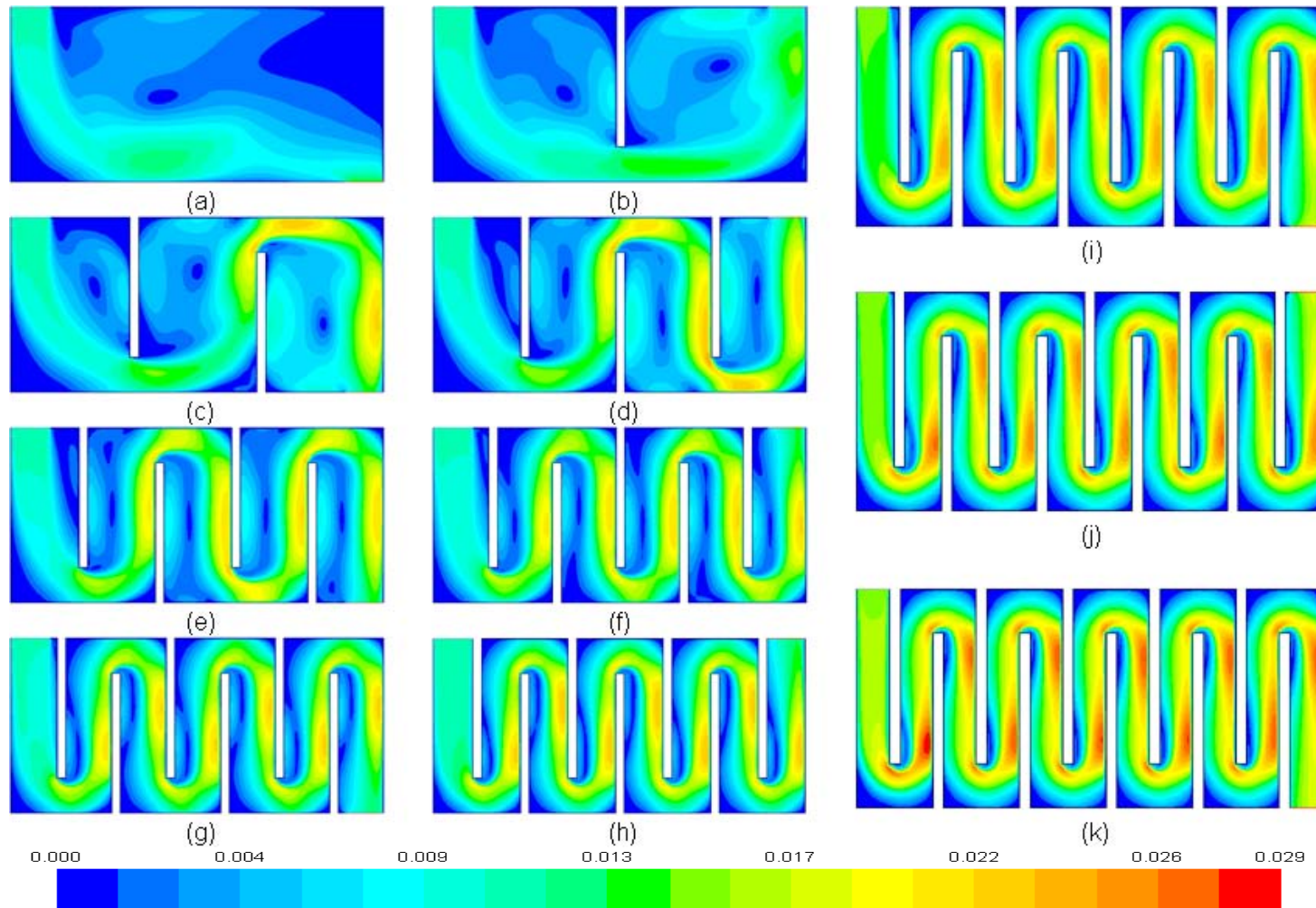
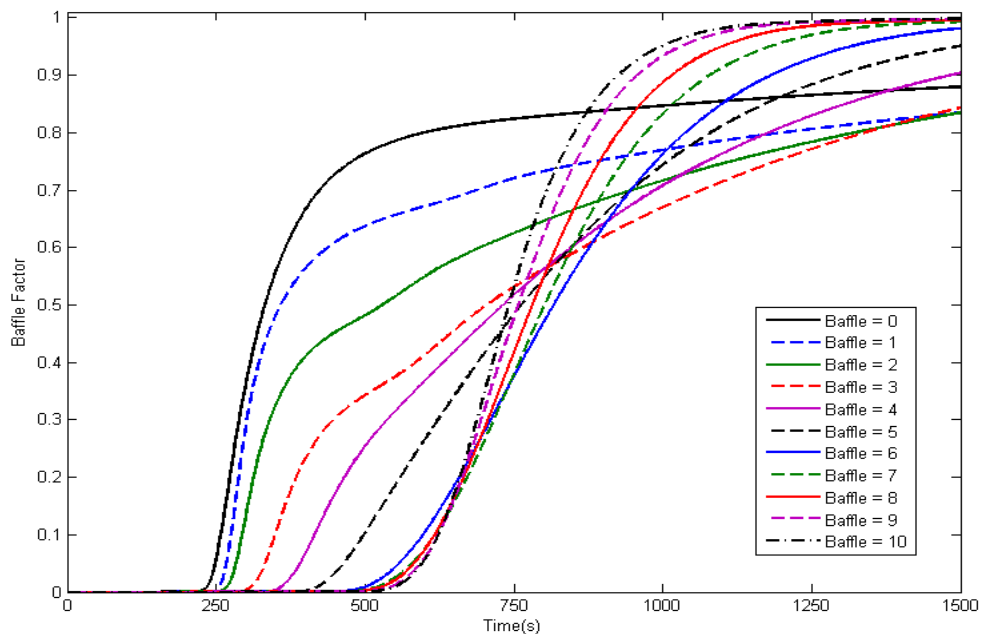
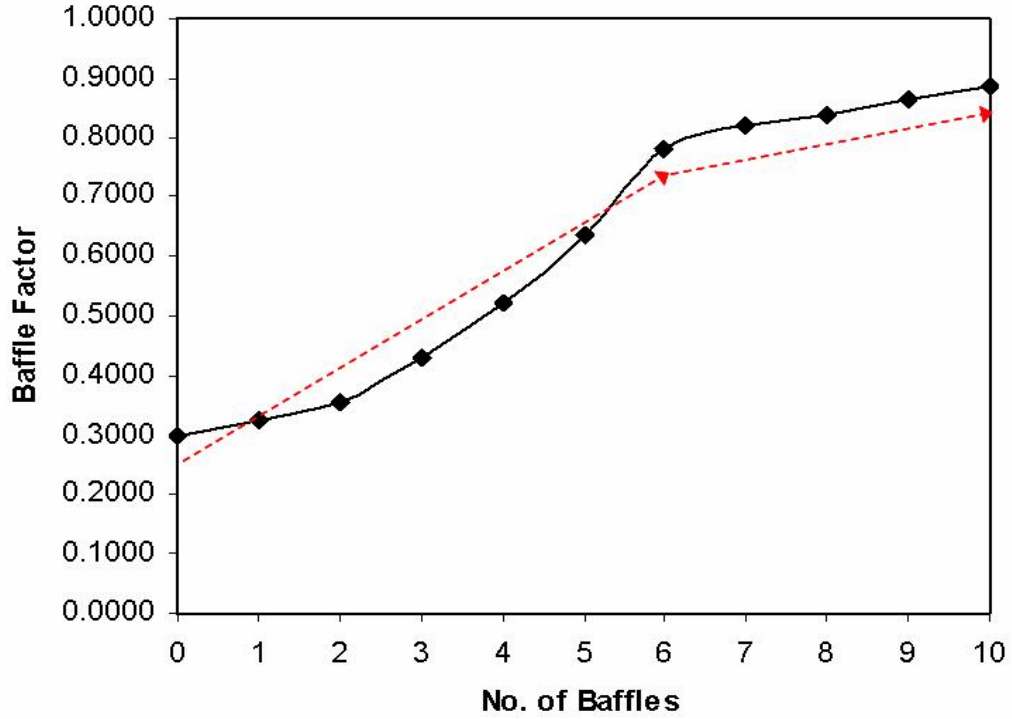


Figure 4.9: Velocity distributions in tanks with different number of baffles:  
 (a) Baffle No. = 0, (b) Baffle No. = 1, (c) Baffle No. = 2, (d) Baffle No. = 3, (e) Baffle No. = 4, (f) Baffle No. = 5, (g) Baffle No. = 6, (h) Baffle No. = 7, (i) Baffle No. = 8, (j) Baffle No. = 0 and (k) Baffle No. = 10. The color bar gives the magnitude of the velocity (in m/s).

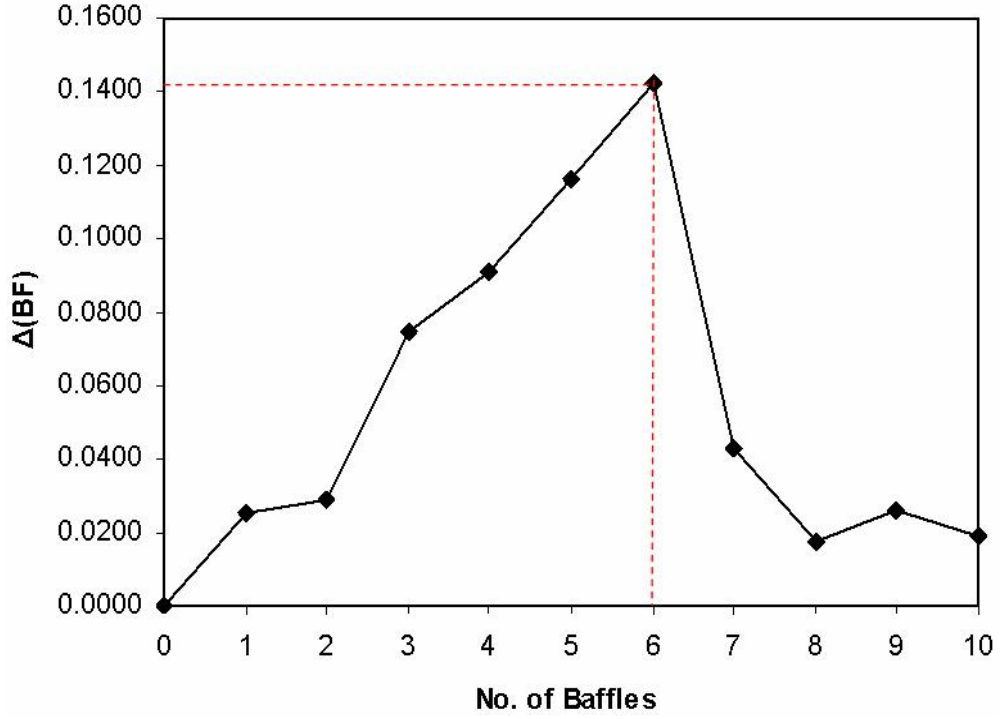
RTD curves for all the 11 baffled configurations are shown in Figure 4.10 (see also Table D.1 in Appendix D for details). The results indicate that the flow becomes less dispersive and approaches plug flow conditions (i.e. the baffle factor increases) as the number of baffles increase as shown in Figure 4.11(a). However, it is not intuitively obvious from the RTD curves and/or the baffle factors whether there is an optimum number of baffles that maximizes plug flow conditions and beyond which diminishing returns begins to occur in the context of hydraulic efficiency. If we calculate the incremental change in the baffle factor with respect to the number of baffles, a better picture emerges as shown in Figure 4.11(b). A clear peak occurs when the number of baffles equals to 6, beyond which the rate of gain in baffle factor goes down (i.e. diminishing returns has set in). Based on this investigation, it appears that the optimum number of baffles is 6 to get the most efficient hydraulic system.



**Figure 4.10: Simulated RTD curves of normalized tracer concentrations at the outlet with baffle numbers from 0 to 10 for a step trace input at the inlet.**



(a)



(b)

Figure 4.11: (a) Baffle factors as a function of the number of baffles; (b) The change in baffle factor as a function of number of baffles.



#### 4.4.4 Dead zone predictions

Using Equation (3.2), we could easily calculate the  $T_m$  from the RTD curve simulated by FLUENT. Figure 12(a) shows the relationship between  $T_m$  and theoretical residence time  $T$ . From  $T_m$ , the efficient mean volume ( $V_m$ ) of the tank can be calculated. The theoretical volume  $V$  is simply the total volume of the tank minus the volume taken by baffles.  $V$  minus  $V_m$  is a measure of the volume of dead zones inside the tank. Table 4.2 shows these results for all the eleven configurations studied here. Figure 4.12(a) and Figure 4.12(b) are figures based on the values shown in Table 4.2. It can be seen that when the number of baffles is equal to 6, the volume of dead zones in the contact tank is minimized. For the same 6-baffled tank, the difference between  $T$  and  $T_m$  is a minimum, which also provides a good indication that the available volume of the tank has been most efficiently used.

**Table 4.2: Dead zone predictions.**

No. of baffles	0	1	2	3	4	5	6	7	8	9	10
$T_m$ (s)	375	504	592	675	669	685	724	709	690	672	660
$T$ (s)	859	844	828	813	797	782	766	751	735	720	704
$Dt$ (s)	484	339	236	138	128	97	42	42	46	48	45
$V_m$ (m <sup>3</sup> )	0.45	0.61	0.71	0.81	0.80	0.82	0.87	0.85	0.83	0.81	0.79
$V$ (m <sup>3</sup> )	1.01	0.99	0.97	0.95	0.93	0.91	0.90	0.88	0.86	0.84	0.82
$dv$ (m <sup>3</sup> )	0.555	0.382	0.258	0.141	0.130	0.093	0.027	0.028	0.033	0.036	0.033

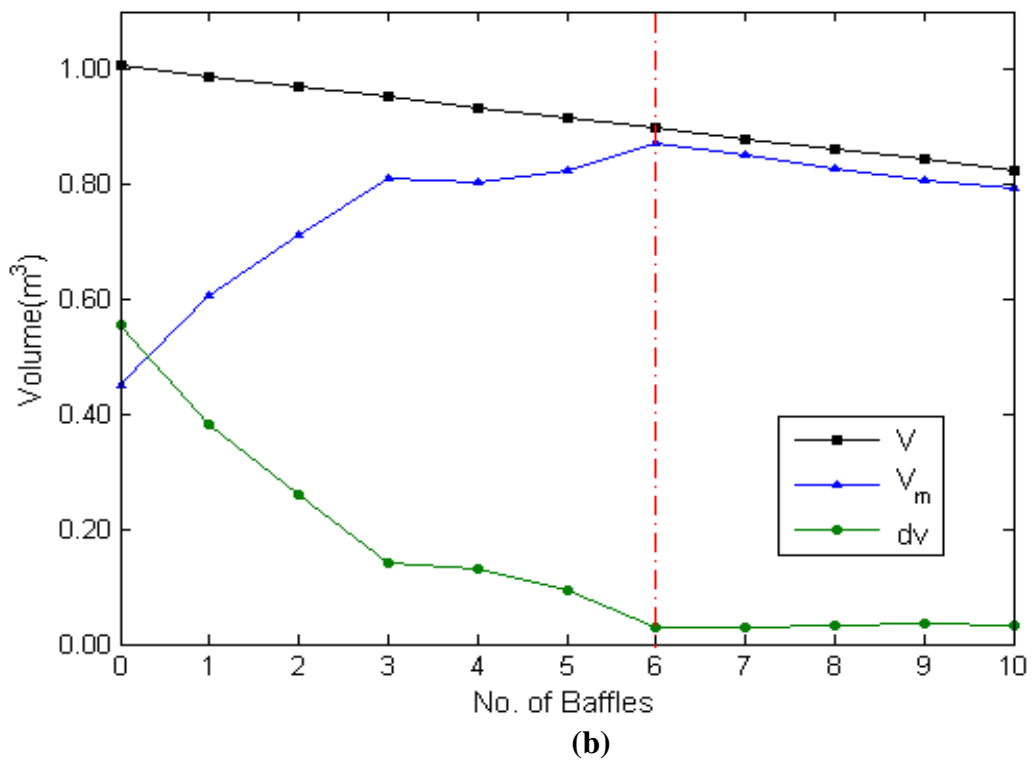
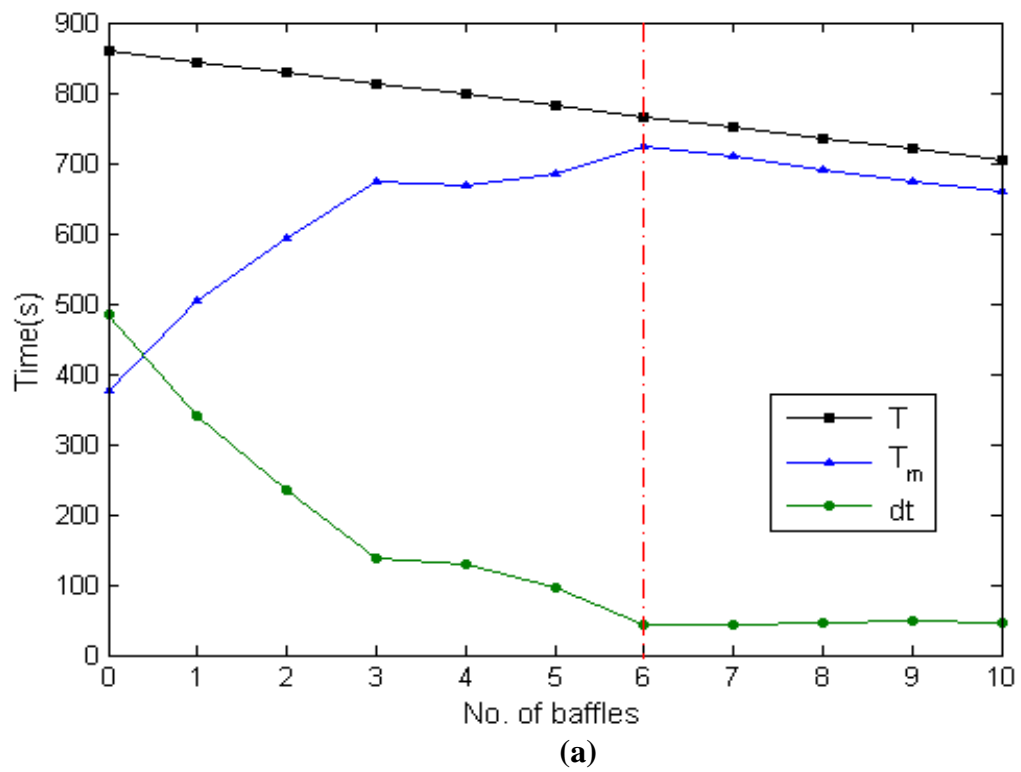


Figure 4.12: (a)  $T_m$ ,  $T$  and  $dt$  values as a function of the number of baffles; (b)  $V$ ,  $V_m$  and  $dv$  values as a function of the number of baffles.

#### 4.4.5 Flow rate vs. baffle factor

Having determined six as the optimum number of baffles for this given footprint, the dependence of the baffle factor as a function of flow rates for the six baffle tank is investigated next.

The original flow rate is  $Q_0 = 0.0017 \text{ m}^3/\text{s}$  as presented before. The velocity fields are simulated by FLUENT with flow rates at the inlet increasing from  $0.6Q_0$ ,  $0.8Q_0$ ,  $Q_0$  to  $1.2Q_0$ , which are flow rates that are typically used when conducting full scale tracer studies. It is easy to see from Figure 4.13 that the flow is more turbulent as the flow rate increases. However, it turns out that the baffle factors are not strongly sensitive to the flow rates as shown in Figure 4.14 where time has been non-dimensionalized using the theoretical hydraulic retention time  $T$ .

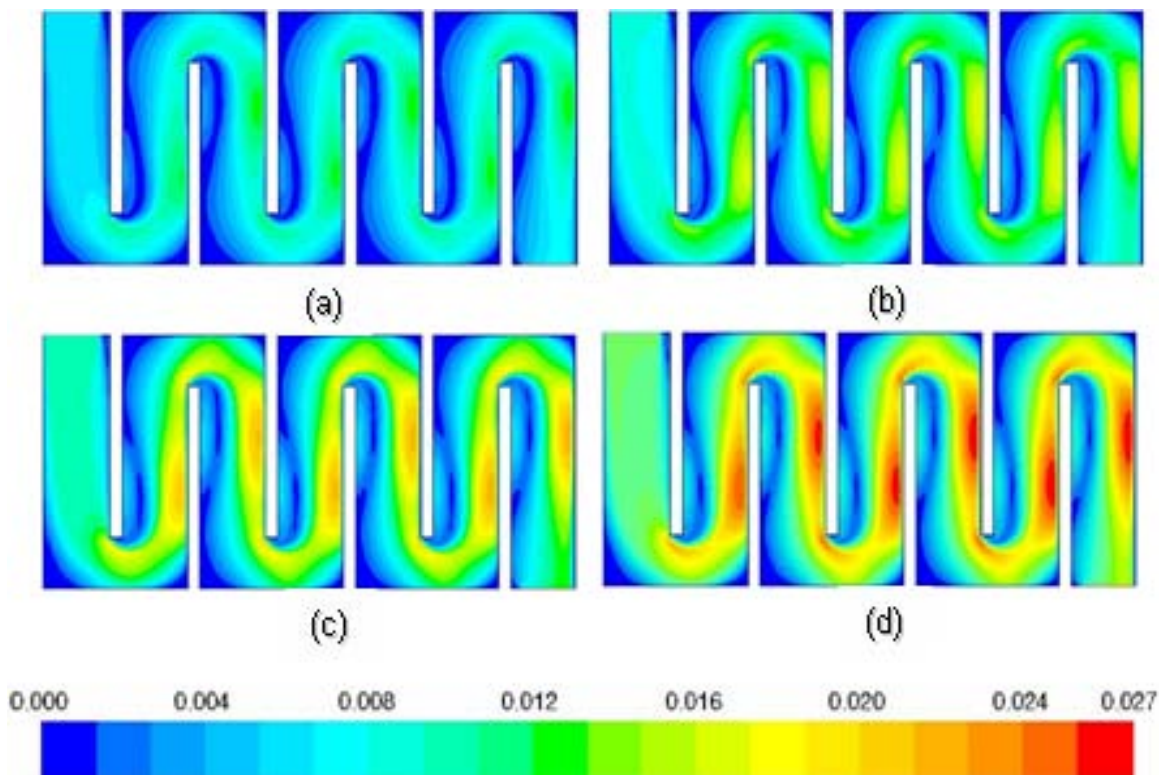


Figure 4.13: Velocity contours with different flow rates at the inlet. (Color bar unit: m/s). (a)  $Q_a = 0.6Q_0$ ; (b)  $Q_b = 0.8Q_0$ ; (c)  $Q_c = Q_0$ ; (d)  $Q_d = 1.2Q_0$ .

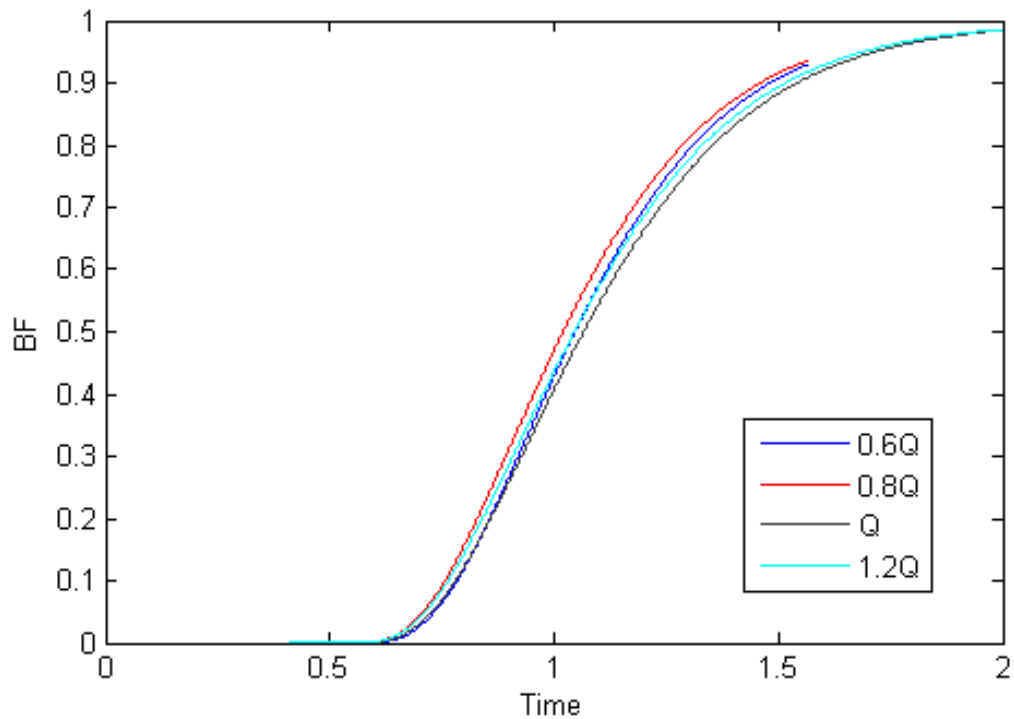


Figure 4.14 Baffle factors as a function of flow rate for the six-baffled tank.

#### 4.5 Conclusions

Model predictions for the velocity field were verified against experimental measurements. The emphasis of this study was to investigate the hydraulic efficiency of baffled tanks for a given footprint as a function of the number of baffles while keeping other relevant variables such as tank size, flow rate etc. constant. Our analysis of RTD curves obtained for total 11 different number of baffles for the same tank indicate there is an optimum number of baffles for which near plug flow conditions are maximized. In addition, results show that for the optimum tank, the volume of dead zones is a minimum, which could be also translated as: for the optimum tank, the value of mean flow through time  $T_m$  is the closest to theoretical hydraulic residence time  $T$ . An extended study using

variation of volume flow rates at the inlet of the optimum tank shows that the inlet flow rate does not alter the hydraulic efficiency significantly.

As discovered from the results of the tracer studies performed by Marske and Boyle (1973), the effectiveness of baffling in achieving a high  $T_{10}/T$  is more related to the geometry and baffling conditions rather than on the particular types of contact basins. Conclusions made here for disinfection tanks should be applicable to water tanks with functions where mixing is important.

A further extension of this work is required to gain insights on how to optimize both the placement and shapes of baffles in disinfection contact times. Such an exercise is feasible using CFD simulations and is likely to provide insights on efficient design of disinfection contact tanks for drinking water systems.

## **CHAPTER 5 SUMMARY AND CONCLUSIONS**

### **5.1 Summary of investigations**

In this thesis, internal hydraulic efficiency has been studied using computational fluid dynamics (CFD). The main results of this research have been presented in Chapter 3 and Chapter 4.

Firstly, in Chapter 3, a study of a previous publication on CFD applications in water treatment tanks explained in detail on how CFD works. A discussion on how to simulate the tracer was provided to show how RTD curves can be obtained from CFD simulations and on how CFD can be use to investigate the internal hydraulics inside a tank.

Secondly, Chapter 4 presents a novel study on understanding the internal hydraulic efficiency of baffled disinfection contact tanks and highlights the value of CFD in improving hydraulic design characteristics of water treatment structures.

### **5.2 Main conclusions**

A FLUENT-based mathematical model incorporating the  $k-\varepsilon$  turbulence model was applied to predict time-averaged velocity fields and a tracer dispersion profile in a water tank. We have presented the results from highly resolved two-dimensional CFD simulations of turbulent mixing and transport in a passive tracer in different model tanks.

Model predictions were verified against experimental measurements. Simulation results on the distribution of the velocity field showed that there were stagnant regions on the back sides of the baffles where tracers were unable to mix.

The emphasis of this study was to investigate the hydraulic efficiency of baffled tanks for a given footprint as a function of the number of baffles while keeping other relevant variables such as tank size, flow rate etc. constant. CFD simulation was applied to increase the design efficiency of the given footprint. Our analysis of RTD curves obtained for total 11 different numbers of baffles for the same tank indicates there is an optimum number of baffles for which near plug flow conditions is maximized. Furthermore, the effect of dead zones on the hydraulic efficiency were quantified and correlated to the flow through times.

### **5.3 Suggestions for future research**

This thesis has only focused on the internal hydraulics inside baffled contact tanks, which allowed for an understanding at a relatively simple level. Further extensions of this research are therefore required and feasible using CFD simulations. Such an extension is likely to provide insights on efficient design of disinfection contact tanks for drinking water systems. Some specific suggestions for further research include:

- When designing a full-scale disinfection tank, the designer should consider the number of baffles, the length to width (L/W) ratio of the baffles, and bend width in order to maximize the tank performance.

- Laboratory experiments should be carried out with modifications to the CFD designs. Study should be extended to include chemical decay of the tracer.

- Use of 3D simulations instead of 2D simulations will make the study more complex but will help in understanding the three-dimensional flow features inside tank.

The remainder of this thesis consists of appendices and references referred to in the previous chapters.

## REFERENCES

- Crozes, G. F., Hagstrom, J. P., Clark, M. M., Ducoste, J. & Burns, C. (1999). Improving clearwell design for CT compliance, *America Water Works Association Research Foundation & America Water Works Association*, Denver, Colorado: 154.
- Craig L. (2005). An overview of USEPA research on remote monitoring and control technology for small drinking water treatment systems, *Patterson*.
- Ducoste, J., Carlson, K. & Bellamy, W. (2001). The integrated disinfection design framework approach to reactor hydraulics characterization, *J. Water Supply Res. Technol. AQUA*, 50 (4): 245–261.
- Falconer, R.A. & Tebbutt, T.H.Y. (1986). A theoretical and hydraulic model study of a chlorine contact tank, *Proc. ICE*, 2 (81): 255–276.
- Falconer, R. A. & Liu, S. Q. (1987). Mathematical model study of plug flow in a chlorine contact tank, *Journal Water Environmental Management*, 1(3): 279-290.
- Falconer, R. A. & Liu, S. Q. (1988). Modeling solute transport using QUICK scheme, *Journal of Environmental Engineering ASCE*, 114(1): 3–20.
- Falconer, R. A. & Ismail, A. I. B. M. (1997). Numerical modeling of tracer transport in a contact tank, *Environmental Int.*, 23(6): 763–773.
- Faust, S. D. & Ally, O. M. (1999). Chemistry of water treatment, 2<sup>nd</sup> ed. *CRC Press*.
- Ford, T. (2005). Protecting public health in small water system - report of an international colloquium. Bozeman, Montana, USA.
- Grayman, W. M., Deininger, R. A., Green, A., Boulos, P. F., Bowcock, R. W. & Godwin, C. C. (1996). Water quality and mixing models for tanks and reservoirs, *Journal of America Water Works Association*, 88(7): 60–73.
- Greene, D. J., Farouk, B. C. & Haas, N. (2004). CFD design approach for chlorine disinfection processes, *Journal of America Water Works Association*, 96(8): 138–150.
- Gualtieri, C. (2004). Analysis of the Effect of Baffles Number on Contact Tank Efficiency with Multiphysics 3.3. *COMSOL Users Conference*, Grenoble.
- Gualtieri, C. (2003). Numerical simulation of flow and tracer transport in a disinfection contact tank, *Hydraulic and Environmental Engineering Department Girolamo Ippolito*.
- Hannoun, I. A., Boulos, P. F. (1997). Optimizing distribution storage water quality: a hydrodynamic approach, *Application Mathematics Model*, 21: 495–502.
- Hannoun, I. A., Boulos, P. F. & List, E. J. (1998) Using hydraulic modeling to optimize contact time. *Journal of America Water Works Association*, August: 77-78.
- Huang, T. H., Brouckaert, C. J., Pryor, M. & Buckley, C. A. (2004). Application of computational fluid dynamics modeling to an ozone contactor, *Water SA*, 30(1): 51–56.

- Kim, Y., et al. (2007). Application of Computational Fluid Dynamics for Optimal Design of Horizontal-Flow Baffled-Channel Powdered Activated Carbon Contactors, *Environmental Engineering Science*, 26: 103-109.
- Kolmogorov, A. N. (1942). "Equations of Turbulent Motion of an Incompressible Fluid," *Izvestia Academy of Sciences, USSR; Physics*, 6(1, 2): 56-58.
- Lauder, B. E. & Sharma, B. I. (1974). "Application of the Energy Dissipation Model of Turbulence to the Calculation of Flow Near a Spinning Disk," *Letters in Heat and Mass Transfer*, 1(2): 131-138.
- Marske, D. M. & Boyle, J. D. (1973). Chlorine contact chamber design-a field evaluation. *Water and Sewage Works*.
- Peplinski, D. K. & Ducoste, J. J. (2002). Modeling of disinfection contactor hydraulics under uncertainty, *Journal of Environmental Engineering ASCE*, 128(11): 1056–1067.
- Rauen, W. B., Lin, B., Falconer, R. A. & Teixeira, E. C. (2008). CFD and experimental model studies for water disinfection tanks with low Reynolds number flows, *Chemical Engineering Journal*, 137: 550-560.
- Rodi, W. (1998). Turbulence models and their application in hydraulics – A state of the art review. Proc., IAHR-Sect. on Fundamentals of Div. II: Experimental and Math. *Fluid Dynamics*.
- Saffman, P. G. (1970). A Model for Inhomogeneous Turbulent Flow, *Process Research Society*, A317: 417-433.
- Shiono, K., Teixeira, E. C. & Falconer, R. A. (1991). Turbulent measurements in chlorine contact tank. *First international conference on water pollution: Modeling, measuring and predicting*, Southampton, UK: 519–531.
- Shiono, K. & Teixeira, E. C. (2000). Turbulent characteristics in a baffled contact tank, *Journal of Hydraulic Research*, 38(6): 403-416.
- Stamou, A. I. (2002). Verification and application of a mathematical model for the assessment of the effect of guiding walls on the hydraulic efficiency of chlorination tanks, *Journal of Hydrology information*, 4(4): 245–254.
- Stovin, V. R. & Saul, A. J. (1998). A computational fluid dynamics (CFD) particle tracking approach to efficiency prediction, *Water Science and Technology*, 37: 285-293.
- Teixeira, E. C. (1993). Hydrodynamic processes and hydraulic efficiency of chlorine contact units. Ph.D Thesis, University of Bradford, UK.
- Templeton, M. R., Hofmann, R. & Andrews, R. C. (2006). Case study comparisons of computational fluid dynamics (CFD) modeling versus tracer testing for determining clearwell residence times in drinking water treatment. *Journal Environment Engineering Science*, 5: 529-536.
- Thayanithy, M. (1984). Hydraulic design aspects of chlorine contact tank, M.Sc. Dissertation, University of Birmingham, U.K.
- USEPA (1999). Disinfection, Profiling and Benchmarking Guidance Manual. United States Environmental Protection Agency (EPA) Office of Water.
- USEPA. National Center for Environmental Research. <http://es.epa.gov/ncer/>
- USEPA. National Primary Drinking Water Regulations: Ground Water Rule. <http://www.epa.gov/EPA-WATER/2000/May/Day-10/w10763.htm>

- USEPA (2000). Report of the national drinking water advisory council small water systems implementation working group.
- USEPA. Safe Drinking Water Act (SDWA).  
<http://www.epa.gov/safewater/sdwa/30th/factsheets/treatment.html#8>
- USEPA (2004). Drinking Water Treatment document.  
[http://www.epa.gov/ogwdw000/sdwa/pdfs/fs\\_30ann\\_treatment\\_web.pdf](http://www.epa.gov/ogwdw000/sdwa/pdfs/fs_30ann_treatment_web.pdf)
- USEPA (2003). Safe Drinking Water Act Amendments of 1996 and Understanding the Safe Drinking Water Act.
- USEPA (1993). Small Public Water Systems and Capacity Development.  
<http://www.epa.gov/safewater/smallsystems/index.html>
- Wang, H. & Falconer, R. A. (1998b). Numerical modeling of flow in chlorine disinfection tanks, *Journal of Hydraulic Engineering ASCE*, 124(9): 918-931.
- Wilcox, D. C. (1988a). "Reassessment of the Scale Determining Equation for Advanced Turbulence Models," *American Institute of Aeronautics and Astronautics Journal*, 26(11): 1299-1310.
- Wilcox, D. C. (2006). Turbulence Modeling for CFD, Third Edition, *DCW Industries*.
- Wilcox, D. C. (2007). Basic Fluid Mechanics, Third Edition, *DCW Industries*.
- White, G. C. (1998). Handbook of Chlorination and Alternative Disinfectants, 4<sup>th</sup> ed., *John Wiley & Sons*.
- Xu, Q., Wilson, J. & Venayagamoorthy, S. K. (2010). Internal Hydraulics of baffled disinfection contact tanks, *Journal of Environmental Engineering ASCE*, submitted.
- Xu, Q. & Venayagamoorthy, S. K. (2010). Hydraulic Efficiency of Baffled Disinfection Contact Tanks, accepted for presentation at *the 6<sup>th</sup> International of Symposium Environmental Hydraulics*, Athens, Greece, 23-25 Jun 2010.

**APPENDIX A – FLUORIDE AND LITHIUM TRACER STUDY PROTOCOL**

**Fluoride and Lithium Tracer Study Protocol**

Jordan Wilson  
Graduate Research Assistant  
Dept. of Civil and Environmental Engineering  
Colorado State University

Qing Xu  
Graduate Research Assistant  
Dept. of Civil and Environmental Engineering  
Colorado State University

Dr. Karan Venayagamoorthy  
Assistant Professor  
Dept. of Civil and Environmental Engineering  
Colorado State University

Prepared for:

Colorado Department of Public Health and Environment  
Water Quality Control Division

## Objective

The objective of the tracer study is to determine the HRT of the studied system.

## Protocol

- 1) Determine flow rate for analysis
  - a. Set flow rate using PID controller

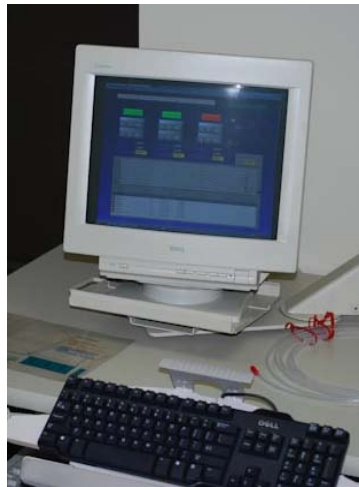


Figure 1 - PID Controller Interface

- b. Verify flow rate with drawdown column

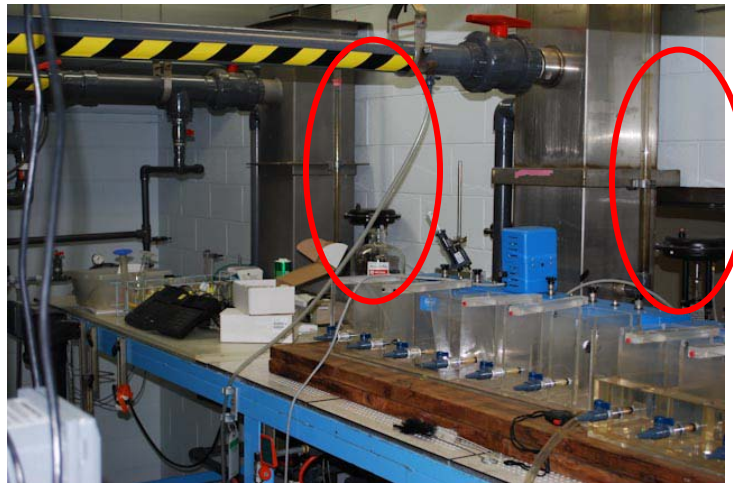


Figure 2 - Drawdown Columns

- 2) Determine system HRT
  - a.  $HRT = \text{System Volume} \div \text{Flow Rate}$



**Figure 3 - Measuring Pipe Loop System**

- 3) Development of sampling protocol
  - a. The sampling protocol is largely dependent on the type of system analyzed
    - i. For a pipe loop configuration (i.e. plug flow), the sampling interval should be 30 seconds within  $\pm 5$  minutes of HRT and 5 minutes within  $\pm 20$  minutes of HRT
    - ii. For baffled basin (i.e. series tank), the sampling interval should be 5 minutes within  $\pm 30$  minutes of HRT and 10 minutes within  $\pm 60$  minutes of HRT
    - iii. For open basin, the sampling interval should be 10 minutes with  $\pm 90$  minutes of HRT
- 4) Sample water to determine chlorine and lithium background levels
- 5) Determine injection and sampling points
  - a. The injection point will be comprised of a 3/8 inch quick-connect fitting to accept the effluent hose from the injection pump



**Figure 4 - Injection Point**

- b. The sampling point should be easily accessible and contain a quarter-turn valve for ease of sampling



**Figure 4 - Sampling Point**

- 6) Set and calibrate injection pump
  - a. Fill bulk container with deionized water and attach to injection pump
  - b. Attach effluent hose from injection pump to the system injection point



**Figure 5 - Pump Attached to DI Water for Calibration**

- c. Open valve to fill the calibration column, then close the valve



**Figure 6 - Pump Calibration Column**

- d. Set pump stroke to 100 and speed to 80



**Figure 7 - Pump Settings**

- e. Turn pump on
  - f. Open valve from calibration column to pump
  - g. Time the drop in the column over a determine volume
  - h. Turn off pump
  - i. Calculate injection flow rate
- 7) Prepare tracer solution



Figure 8 - Tracer Compounds (LiCl & NaF)

- a. Determine the volume of tracer solution needed
  - i.  $Volume_{tracer} = Mean\ Resonance\ Time \times Injection\ Pump\ Rate$
- b. Determine the mass of *LiCl* added to tracer solution (Assume a system maximum of 0.04 mg/L based on background levels)
  - i.  $\frac{0.04\ mg\ Li}{L} \times Volume_{system} = mass_{Li}$
  - ii.  $mass_{LiCl} = mass_{Li} \times \frac{42.394\ g\ LiCl}{6.941\ g\ Li}$
- c. Determine the mass of *NaF* added to tracer solution (Assume a system maximum of 1.00 mg/L based on background levels)
  - i.  $\frac{1.0\ mg\ F}{L} \times Volume_{system} = mass_F$
  - ii.  $mass_{NaF} = mass_F \times \frac{41.99\ g\ NaF}{18.998\ g\ F}$
- d. Add the dry masses of *LiCl* and *NaF* to the determined volume of water in a) and mix well



Figure 9 - Thoroughly Mixing Tracer Solution

- 8) Attach bulk tracer solution to injection pump



Figure 10 - Injection Pump Connected to Tracer Solution

- 9) Turn on injection pump
  - a. Allow for 2 minutes to pass allowing for the tracer to reach the injection point
- 10) Sample at intermediate point to determine maximum tracer concentration in system



Figure 11 - Intermediate Sampling Point

- 11) Sample according to protocol
  - a. Label containers appropriately
  - b. Place adequate sample in test tube for laboratory analysis of lithium
  - c. Place adequate sample in open container for on-site analysis of fluoride
- 12) Analyze chlorine using colormeter
  - a. Place an adequate amount of DI water in an open container
  - b. Insert AccuVac sample and break off glass tip



Figure 12 - Sealed AccuVac Samplers

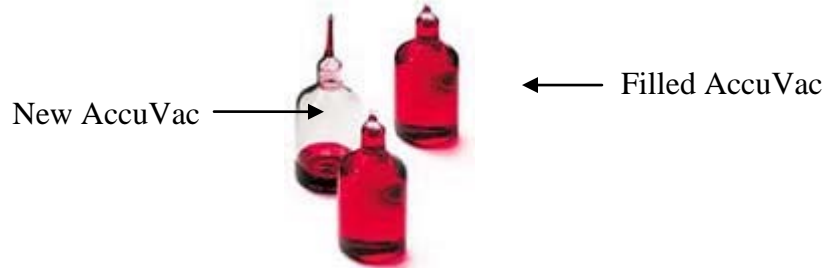


Figure 13 - AccuVac Sampler

- c. Turn on colormeter



Figure 14 - DR890 Colormeter

- d. Program – 28 – enter
- e. Remove colormeter cover, insert DI water AccuVac sample, replace cover, and press zero

- f. Place new AccuVac into sample container, break off glass tip, press timer – enter on colormeter
  - g. When alarm sounds, remove colormeter cover, insert AccuVac sample, replace cover, press read, and record reading
  - h. Repeat steps 12.f and 12.g for remaining samples
- 13) Review results
- a. Analyze colormeter fluoride results to ensure samples captured tracer breakthrough
- 14) Adjust sampling protocol (if necessary)
- 15) Repeat steps 3-12 (if necessary)
- 16) Repeat procedure (steps 1-15) for all flowrates to be analyzed

## APPENDIX B –

### DERIVATION OF REYNOLDS STRESS AND RANS EQUATIONS

#### Derivation of Reynolds Stress

In fluid dynamics, the Reynolds stresses is the stress tensor in a fluid due to the random turbulent fluctuations in fluid momentum. The stress is obtained from an average (typically in some loosely defined fashion) over these fluctuations.

To illustrate, here we use Cartesian vector index notation. For simplicity, consider an incompressible fluid:

Given the fluid velocity  $u_i$  as a function of position and time, write the average fluid velocity as  $\overline{u_i}$ , and the velocity fluctuation is  $u'_i$ . Then  $u_i = \overline{u_i} + u'_i$ .

The conventional ensemble rules of averaging are that

$$\begin{aligned}\overline{\overline{a}} &= \overline{a} \\ \overline{a + b} &= \overline{a} + \overline{b} \\ \overline{ab} &= \overline{a}\overline{b}\end{aligned}$$

One splits the Euler equations or the Navier-Stokes equations into an average and a fluctuating part. One finds that upon averaging the fluid equations, a stress on the right hand side appears of the form  $\overline{\rho u'_i u'_j}$ . This is the Reynolds stress, conventionally written  $R_{ij}$ :

$$R_{ij} \equiv \overline{\rho u'_i u'_j}$$

The divergence of this stress is the force density on the fluid due to the turbulent fluctuations.

For instance, for an incompressible, viscous, Newtonian fluid, the continuity and momentum equations can be written as

$$\frac{\partial u_i}{\partial x_i} = 0$$

and

$$\rho \frac{Du_i}{Dt} = -\frac{\partial p}{\partial x_i} + \mu \left( \frac{\partial^2 u_i}{\partial x_j \partial x_j} \right),$$

where  $D / D_t$  is the Lagrangian derivative or the Substantial derivative,

$$\frac{D}{Dt} = \frac{\partial}{\partial t} + u_j \frac{\partial}{\partial x_j}.$$

Defining the flow variables above with a time-averaged component and a fluctuating component, the continuity and momentum equations become

$$\frac{\partial (\bar{u}_i + u'_i)}{\partial x_i} = 0,$$

and

$$\rho \left[ \frac{\partial (\bar{u}_i + u'_i)}{\partial t} + (\bar{u}_j + u'_j) \frac{\partial (\bar{u}_i + u'_i)}{\partial x_j} \right] = -\frac{\partial (\bar{p} + p')}{\partial x_i} + \mu \left[ \frac{\partial^2 (\bar{u}_i + u'_i)}{\partial x_j \partial x_j} \right].$$

Examining one of the terms on the left hand side of the momentum equation, it is seen that

$$(\bar{u}_j + u'_j) \frac{\partial (\bar{u}_i + u'_i)}{\partial x_j} = \frac{\partial (\bar{u}_i + u'_i) (\bar{u}_j + u'_j)}{\partial x_j} - (\bar{u}_i + u'_i) \frac{\partial (\bar{u}_j + u'_j)}{\partial x_j},$$

where the last term on the right hand side vanishes as a result of the continuity equation. Accordingly, the momentum equation becomes

$$\rho \left[ \frac{\partial (\bar{u}_i + u'_i)}{\partial t} + \frac{\partial (\bar{u}_i + u'_i) (\bar{u}_j + u'_j)}{\partial x_j} \right] = -\frac{\partial (\bar{p} + p')}{\partial x_i} + \mu \left[ \frac{\partial^2 (\bar{u}_i + u'_i)}{\partial x_j \partial x_j} \right].$$

Now the continuity and momentum equations will be averaged. The ensemble rules of averaging need to be employed, keeping in mind that the average of products of fluctuating quantities will not in general vanish. After averaging, the continuity and momentum equations become

$$\frac{\partial \bar{u}_i}{\partial x_i} = 0,$$

and

$$\rho \left[ \frac{\partial \bar{u}_i}{\partial t} + \frac{\partial \bar{u}_i \bar{u}_j}{\partial x_j} + \frac{\partial \overline{u'_i u'_j}}{\partial x_j} \right] = -\frac{\partial \bar{p}}{\partial x_i} + \mu \frac{\partial^2 \bar{u}_i}{\partial x_j \partial x_j}.$$

Dividing both sides of the momentum equation by  $\rho$  yields

$$\frac{\partial \bar{u}_i}{\partial t} + \frac{\partial \bar{u}_i \bar{u}_j}{\partial x_j} + \frac{\partial \overline{u'_i u'_j}}{\partial x_j} = -\frac{1}{\rho} \frac{\partial \bar{p}}{\partial x_i} + \nu \frac{\partial^2 \bar{u}_i}{\partial x_j \partial x_j}.$$

Using the chain rule on one of the terms of the left hand side, it is revealed that

$$\frac{\partial \overline{u_i u_j}}{\partial x_j} = \overline{u_j} \frac{\partial \overline{u_i}}{\partial x_j} + \overline{u_i} \frac{\partial \overline{u_j}}{\partial x_j},$$

where the last term on the right hand side vanishes as a result of the averaged continuity equation. The averaged momentum equation now becomes

$$\frac{\partial \overline{u_i}}{\partial t} + \overline{u_j} \frac{\partial \overline{u_i}}{\partial x_j} + \frac{\partial \overline{u'_i u'_j}}{\partial x_j} = -\frac{1}{\rho} \frac{\partial \overline{p}}{\partial x_i} + \nu \frac{\partial^2 \overline{u_i}}{\partial x_j \partial x_j}.$$

This equation can be rearranged to arrive at a well-known form,

$$\frac{\partial \overline{u_i}}{\partial t} + \overline{u_j} \frac{\partial \overline{u_i}}{\partial x_j} = -\frac{1}{\rho} \frac{\partial \overline{p}}{\partial x_i} + \frac{1}{\rho} \frac{\partial}{\partial x_j} \left( \mu \frac{\partial \overline{u_i}}{\partial x_j} - \overline{\rho u'_i u'_j} \right),$$

where the Reynolds stresses,  $\overline{\rho u'_i u'_j}$ , are collected with the traditional normal and shear stress terms,  $\mu \frac{\partial \overline{u_i}}{\partial x_j}$ .

The question then is what is the value of the Reynolds stress? The problem is recognized as a closure problem. A transport equation for the Reynolds stress may be found by taking the outer product of the fluid equations for the fluctuating velocity, with itself.

One finds that the transport equation for the Reynolds stress includes terms with higher-order correlations (specifically, the triple correlation  $\overline{v'_i v'_j v'_k}$ ) as well as correlations with pressure fluctuations (i.e. momentum carried by sound waves). A common solution is to model these terms by simple ad-hoc prescriptions.

## Derivation of RANS Equations

The basic tool required for the derivation of the RANS equations from the instantaneous Navier–Stokes equations is the Reynolds decomposition. Reynolds decomposition refers to separation of the flow variable (like velocity  $u$ ) into the mean (time-averaged) component ( $\overline{u}$ ) and the fluctuating component ( $u'$ ). Thus,

$$u(\mathbf{x}, t) = \overline{u}(\mathbf{x}) + u'(\mathbf{x}, t)$$

where,  $\mathbf{x} = (x, y, z)$  is the position vector.

The following rules will be useful while deriving the RANS. If  $f$  and  $g$  are two flow variables (like density ( $\rho$ ), velocity ( $u$ ), pressure ( $p$ ), etc.) and  $s$  is one of the independent variables ( $x, y, z$ , or  $t$ ) then,

$$\begin{aligned}
\overline{\bar{f}} &= \bar{f} \\
\overline{f + g} &= \bar{f} + \bar{g} \\
\overline{fg} &= \bar{f}\bar{g} \\
\overline{fg} &\neq \overline{f\bar{g}} \\
\frac{\partial \bar{f}}{\partial s} &= \frac{\partial \bar{f}}{\partial s}
\end{aligned}$$

Now the Navier–Stokes equations of motion for an incompressible Newtonian fluid are:

$$\begin{aligned}
\frac{\partial u_i}{\partial x_i} &= 0 \\
\frac{\partial u_i}{\partial t} + u_j \frac{\partial u_i}{\partial x_j} &= f_i - \frac{1}{\rho} \frac{\partial p}{\partial x_i} + \nu \frac{\partial^2 u_i}{\partial x_j \partial x_j}
\end{aligned}$$

Substituting,  $u_i = \bar{u}_i + u'_i$ ,  $p = \bar{p} + p'$ , etc. and taking a time-average of these equations yields,

$$\begin{aligned}
\frac{\partial \bar{u}_i}{\partial x_i} &= 0 \\
\frac{\partial \bar{u}_i}{\partial t} + \bar{u}_j \frac{\partial \bar{u}_i}{\partial x_j} + \overline{u'_j \frac{\partial u'_i}{\partial x_j}} &= \bar{f}_i - \frac{1}{\rho} \frac{\partial \bar{p}}{\partial x_i} + \nu \frac{\partial^2 \bar{u}_i}{\partial x_j \partial x_j}
\end{aligned}$$

The momentum equation can also be written as,

$$\frac{\partial \bar{u}_i}{\partial t} + \frac{\partial \bar{u}_j \bar{u}_i}{\partial x_j} = \bar{f}_i - \frac{1}{\rho} \frac{\partial \bar{p}}{\partial x_i} + \nu \frac{\partial^2 \bar{u}_i}{\partial x_j \partial x_j} - \frac{\partial \overline{u'_i u'_j}}{\partial x_j}$$

On further manipulations this yields,

$$\rho \frac{\partial \bar{u}_i}{\partial t} + \rho \frac{\partial \bar{u}_j \bar{u}_i}{\partial x_j} = \rho \bar{f}_i + \frac{\partial}{\partial x_j} \left[ -\bar{p} \delta_{ij} + 2\mu \bar{S}_{ij} - \rho \overline{u'_i u'_j} \right]$$

where,  $\bar{S}_{ij} = \frac{1}{2} \left( \frac{\partial \bar{u}_i}{\partial x_j} + \frac{\partial \bar{u}_j}{\partial x_i} \right)$  is the mean rate of strain tensor.

Finally, since integration in time removes the time dependence of the resultant terms, the time derivative must be eliminated, leaving:

$$\rho \frac{\partial \bar{u}_j \bar{u}_i}{\partial x_j} = \rho \bar{f}_i + \frac{\partial}{\partial x_j} \left[ -\bar{p} \delta_{ij} + 2\mu \bar{S}_{ij} - \rho \overline{u'_i u'_j} \right]$$

## APPENDIX C – UDF CODE USING IN FLUENT

### DEFINE DIFFUSIVITY

#### *Description*

We use DEFINE DIFFUSIVITY in FLUENT to specify the diffusivity for the user-defined scalar (UDS) transport equations.

#### *Usage*

DEFINE DIFFUSIVITY(name,c,t,i)

#### **Argument Type**

symbol name

cell t c

Thread \*t

int i

#### **Function returns**

real

#### **Description**

UDF name

Cell index

Pointer to cell thread on which the diffusivity function is to be applied

Index that identifies the species or user-defined scalar

There are four arguments to DEFINE DIFFUSIVITY: *name*, *c*, and *t*, and *i*.

We supply *name*, the name of the UDF. *c*, *t*, and *i* are variables that are passed by the FLUENT solver to our UDF. The UDF will need to compute the diffusivity only for a single cell and return the real value to the solver. Since that diffusivity UDFs are called by FLUENT from within a loop on cell threads. Consequently, the UDF will not need to loop over cells in a thread since FLUENT is doing it outside of the function call.

*The UDF code using in Chapter 3 and Chapter 4*

The following UDF, named *diff*, computes the diffusivity for the simulations of this thesis when using a user-defined scalar. Note the calculations do not require that energy,

radiation, or species transport calculations have been performed. This function can be executed as an interpreted or compiled UDF.

```
/******  
UDF that computes diffusivity for mean age using a user-defined scalar.  
*****/  
#include "udf.h"  
DEFINE_DIFFUSIVITY(diff,c,t,i)  
{  
return C_MU_T(c,t) / 0.7+0.001;  
}
```

*Hooking a Diffusivity UDF to FLUENT*

After the UDF is defined using DEFINE DIFFUSIVITY is interpreted, the name that we specified in the DEFINE macro argument (e.g., diff) will become visible and selectable in the Materials panel in FLUENT.

**APPENDIX D – RESULTS TABLE OF CHAPTER 4**

Number of Baffles	0	1	2	3	4	5	6	7	8	9	10
Baffle Area (m <sup>2</sup> )	0.0000	0.0338	0.0675	0.1013	0.1350	0.1688	0.2025	0.2363	0.2700	0.3038	0.3375
Surface Area (m <sup>2</sup> )	1.8753	1.8416	1.8078	1.7741	1.7403	1.7066	1.6728	1.6391	1.6053	1.5716	1.5378
Mean Depth (m)	0.5360	0.5360	0.5360	0.5360	0.5360	0.5360	0.5360	0.5360	0.5360	0.5360	0.5360
Volume (m <sup>3</sup> )	1.0052	0.9871	0.9690	0.9509	0.9328	0.9147	0.8966	0.8785	0.8604	0.8424	0.8243
Flow Rate (m <sup>3</sup> /s)	0.0012	0.0012	0.0012	0.0012	0.0012	0.0012	0.0012	0.0012	0.0012	0.0012	0.0012
<i>HRT</i> (s)	859.11	843.65	828.19	812.73	797.27	781.80	766.34	750.88	735.42	719.96	704.50
<i>T</i> <sub>10</sub> (s)	258	275	294	349	415	498	597	617	617	623	623
<i>T</i> <sub>90</sub> (s)	1923	2373	1980	1793	1484	1295	1182	1080	1015	958	926
Baffle Factor	0.3003	0.3260	0.3550	0.4294	0.5205	0.6370	0.7790	0.8217	0.8390	0.8653	0.8843
<i>T</i> <sub>10</sub> / <i>T</i> <sub>90</sub>	0.1342	0.1159	0.1485	0.1946	0.2796	0.3846	0.5051	0.5713	0.6079	0.6503	0.6728
Δ(BF)		0.0257	0.0290	0.0744	0.0911	0.1165	0.1420	0.0427	0.0173	0.0264	0.0190